Figure 2
Quantitative real-time PCR analysis, macroscopic analysis, and histology of *RAMP2*$^{-/-}$ embryos. (**A**) Gene expression of AM, CRLR, and RAMPs in E13.5 WT and *RAMP2*$^{-/-}$ embryos, assessed by real-time PCR of total RNA. No RAMP2 expression was detected in *RAMP2*$^{-/-}$ mice, confirming *RAMP2* was successfully destroyed. Conversely, RAMP3 expression did not differ between *RAMP2*$^{-/-}$ and WT mice, showing that the absence of RAMP2 did not induce compensatory upregulation of RAMP3 during development. AM expression was upregulated more than 5-fold in *RAMP2*$^{-/-}$ mice. $n = 6$ per group. $^{**}P < 0.01$ vs. WT. (**B–L**) Development of blood vessels in E13.5 WT and *RAMP2*$^{-/-}$ mice. Appearance of the yolk sac (**B**) and vitelline arteries (**C** and **D**). (**E** and **F**) CD31 immunostaining of sections of yolk sacs. Arrows indicate sections of vitelline arteries. (**G** and **H**) Whole-mount immunofluorescence staining of CD31 in yolk sacs. In **C–H**, vitelline arteries were well developed on the yolk sacs of WT mice but poorly developed on those of *RAMP2*$^{-/-}$ mice. (**I–L**) TUNEL staining of sections of vitelline artery (**I** and **J**) and umbilical vessel (**K** and **L**) in E13.5 WT and *RAMP2*$^{-/-}$ embryos. Apoptosis was visualized in green fluorescence. Arrows indicate vessel lumens. Some ECs in *RAMP2*$^{-/-}$ mice were TUNEL positive. (**M** and **N**) Severe systemic edema observed in *RAMP2*$^{-/-}$. Front (**M**) and side (**N**) views of WT and *RAMP2*$^{-/-}$ embryos at midgestation. Some *RAMP2*$^{-/-}$ embryos showed severe systemic edema. (**O–R**) Pericardial effusion in *RAMP2*$^{-/-}$ mice. (**O** and **P**) Magnified side view of embryos at midgestation revealing the appearance of the pericardial space in *RAMP2*$^{-/-}$ embryos. (**Q** and **R**) Sagittal sections showing the pericardial space in embryos at midgestation. The pericardial space was larger in *RAMP2*$^{-/-}$ than WT embryos and showed the accumulation of pericardial effusion. (**S–U**) Severe hemorrhagic changes in *RAMP2*$^{-/-}$ mice. (**S**) Side view of WT and *RAMP2*$^{-/-}$ embryos at midgestation. (**T** and **U**) Sections of the liver at the same stage. Some *RAMP2*$^{-/-}$ embryos showed severe hemorrhagic changes that were apparent on their surface and within the liver. Scale bars: 20 μm (**E** and **F**); 50 μm (**I–L**, **T**, and **U**); 200 μm (**Q** and **R**).

WT, 18.4 ± 1.4 mmHg; *RAMP2*$^{+/-}$, 13.3 ± 1.3 mmHg; $P < 0.05$, $n = 6$ per group). In contrast, CGRP-induced depressor effects did not differ in *RAMP2*$^{+/-}$ and WT mice (maximum percent change in systolic BP, WT, 15.9 ± 1.2 mmHg; *RAMP2*$^{+/-}$, 14.4 ± 1.3 mmHg; NS, $n = 6$ per group). Interestingly, AM expression was significantly upregulated in the aortas of *RAMP2*$^{+/-}$ mice, which suggests that reducing the number of functional AM receptors caused a compensatory upregulation of AM expression and implies that the AM-RAMP2 system is also important in the vascular function of adults. This prompted us to analyze the angiogenic properties of the AM-RAMP2 system in adult mice. We found that aortic ring explants cultured in collagen gel sprouted microvessels when stimulated with VEGF and that this

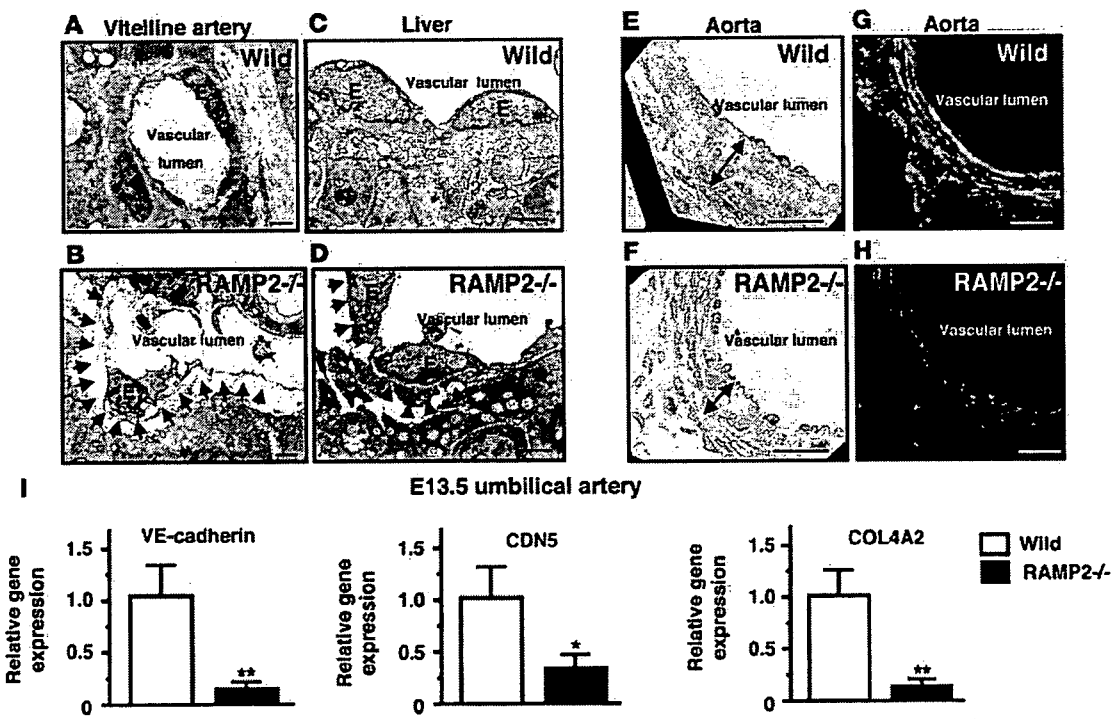

Figure 3
Abnormalities of vascular structure and gene expression in *RAMP2*$^{-/-}$ embryos. (**A–H**) Vascular structure of WT and *RAMP2*$^{-/-}$ embryos. Transmission electron micrographs of vitelline arteries (**A** and **B**), hepatic vessels (**C** and **D**), and aortas (**E** and **F**) from E12.5 *RAMP2*$^{-/-}$ and WT embryos. The vitelline arteries and hepatic vessels from *RAMP2*$^{-/-}$ mice showed the detachment of ECs (E) from basement membrane (arrows, **B** and **D**). In aortas from *RAMP2*$^{-/-}$ mice, the smooth muscle cell layer was thinner and rougher than in aortas from WT mice (double-headed arrows, **E** and **F**). (**G** and **H**) Immunohistochemical staining for type IV collagen and actin in aortas from WT and *RAMP2*$^{-/-}$ mice. Green, immunohistochemical staining using anti–mouse type IV collagen antibody; red, phalloidin (actin); blue, DAPI (nuclei). The structure of the smooth muscle cell layer and the basement membrane showed severe deformity in *RAMP2*$^{-/-}$ mice. (**I**) Quantitative real-time PCR analysis of gene expression in the umbilical artery from E13.5 embryos. Expression levels are shown relative to the level in WT embryos. VE-cadherin, CDN5, and α2 type IV collagen (COL4A2) expression was reduced in arteries from *RAMP2*$^{-/-}$ mice. $n = 6$ per group. $^{*}P < 0.05$, $^{**}P < 0.01$ vs. WT. Scale bars: 2 μm (**A–D**); 25 μm (**E–H**).

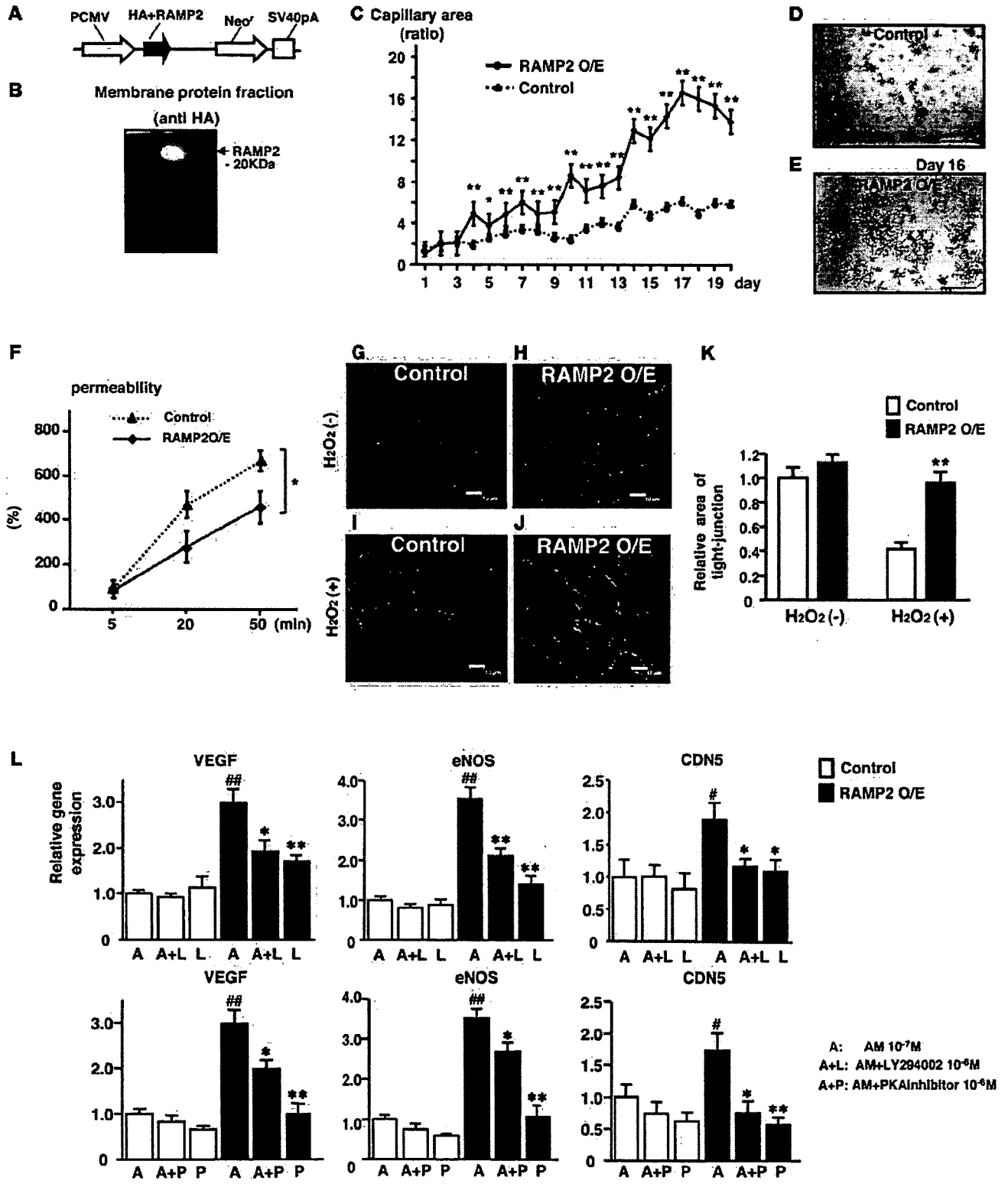
A
PCMV
HA+RAMP2
Neo'
SV40pA
B
Membrane protein fraction
(anti HA)
RAMP2
- 20KDa
C Capillary area
(ratio)
RAMP2 O/E
Control
day
D
Control
E
Day 16
RAMP2 O/E
F
permeability
Control
RAMP2O/E
(%)
(min)
G
Control
H
RAMP2 O/E
I
Control
J
RAMP2 O/E
H2O2 (-)
H2O2 (+)
K
Control
RAMP2 O/E
Relative area of tight-junction
H2O2 (-)
H2O2 (+)
L
VEGF
eNOS
CDN5
Relative gene expression
Control
RAMP2 O/E
A: AM 10-7M
A+L: AM+LY294002 10-6M
A+P: AM+PKAInhibitor 10-6M

Figure 4
Establishment and functional analysis of the RAMP2O/E line. (**A**) Plasmid vector used to overexpress RAMP2 (see Methods). (**B**) Western blot analysis of the membrane protein fraction from RAMP2O/E cells showing expression of the transfected gene. (**C–E**) Capillary formation by EAhy926 cells on Matrigel. RAMP2O/E cells or control ECs were cultured in 24-well culture plates coated with Matrigel in medium containing 10^{-7} M AM, and capillary formation was monitored microscopically. (**C**) Capillary area relative to day-1 cell surface area. RAMP2O/E cells exhibited greater angiogenesis than control. $n = 8$ per group. (**D** and **E**) Representative photomicrographs of RAMP2O/E and control cells. (**F**) In vitro vascular permeability assay (see Methods). The permeability of the monolayer, assessed using a fluorescence microplate reader, is expressed relative to control at 5 min. RAMP2O/E cells showed significantly lower permeability than control ECs. $n = 10$ per group. $^{*}P < 0.05$, $^{**}P < 0.01$ vs. control. (**G–J**) Immunostaining of ZO-1. ECs were cultured until confluent on chamber slides in the presence of 10^{-7} M AM. Two hours after treatment with 0.5 mM H_2O_2, the cells were immunostained using anti–ZO-1 antibody and Hoechst 33342. (**K**) Comparison of the tight junctions illustrated by the immunostaining in **G–J**. Tight junctions were better preserved after H_2O_2 treatment in RAMP2O/E cells than control ECs. $^{**}P < 0.01$ vs. H_2O_2-treated control; comparison in 4 microscopic fields each from 3 independent experiments. (**L**) Quantitative real-time PCR analysis of gene expression in ECs cultured on Matrigel. Values are relative to control ECs treated with 10^{-7} M AM. RAMP2O/E cells showed stronger expression of VEGF, eNOS, and CDN5 than control cells; this effect was blocked by LY294002 (10^{-6} M) or a PKA inhibitor (10^{-6} M). $n = 6$ per group. $^{\#\#}P < 0.01$ and $^{\#}P < 0.05$ vs. AM-treated control. $^{**}P < 0.01$ and $^{*}P < 0.05$ vs. AM-treated RAMP2O/E. Scale bars: 50 μm (**D** and **E**); 10 μm (**G–J**).

angiogenic effect was greatly diminished in explants from *RAMP2*$^{+/-}$ mice (Figure 5, B–E). Similarly, in Matrigel plug assays, *RAMP2*$^{+/-}$ mice showed reduced neovascularization in response to stimulation with bFGF (Figure 5, F and G). We also cultured tissue from the aorta-gonad-mesonephros (AGM) regions of E10.5 embryos, which were plated on mouse OP9 stromal cells to promote angiogenesis. We found that there was substantially less development of a vascular network in tissue from *RAMP2*$^{+/-}$ than WT mice (Figure 5, H and I).

Enhanced vascular permeability in adult RAMP2$^{+/-}$ *mice.* Based on the findings presented thus far, we hypothesized that the AM-RAMP2 system regulates vascular stability in adults as well as during development, which we tested by analyzing vascular permeability in adult *RAMP2*$^{+/-}$ mice. We initially generated a footpad edema model by subcutaneously injecting λ-carrageenan, a sulfated high-MW polygalactan. As expected, *RAMP2*$^{+/-}$ mice showed greater swelling than did WT mice (Figure 6A). We then directly measured vascular permeability using a skin edema model. Mice were injected with FITC-BSA via the tail vein as a tracer of vascular permeability, after which serum exudation caused by subcutaneous injection of histamine was measured using a fluorescence microplate reader. As shown in Figure 6B, *RAMP2*$^{+/-}$ mice exhibited greater vascular permeability than did WT mice.

Finally, to prove that the capacity of the AM-RAMP2 system to regulate vascular permeability could in fact make it a useful therapeutic target, we generated a brain edema model in which edema was caused by injuring the brain using a liquid nitrogen–cooled copper probe. Twenty-four hours after the injury, *RAMP2*$^{+/-}$ mice showed greater vascular permeability than did WT mice (Figure 6C), which suggests that the AM-RAMP2 system is important for maintenance of the blood-brain barrier.

Discussion

The mechanism by which a stable and functional vascular network is generated and regulated by humoral factors is still not fully understood. For example, VEGF alone is insufficient for stable vessel formation (36) and presents major disadvantages for thera-

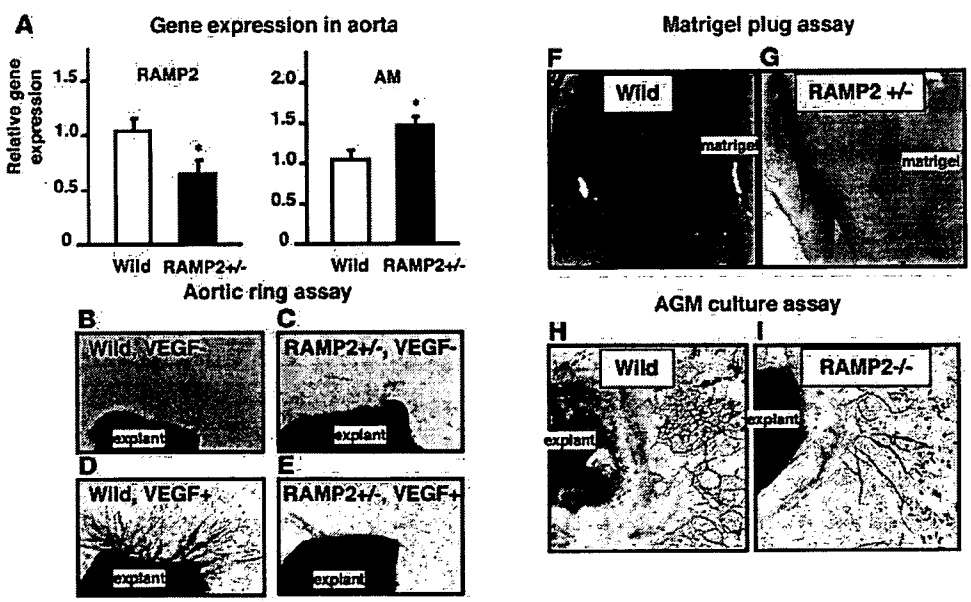

Figure 5
Reduced responses to angiogenic stimuli in adult *RAMP2*$^{+/-}$ mice. (**A**) Gene expression in aortas from 8-week-old WT and *RAMP2*$^{+/-}$ mice. Quantitative real-time PCR analysis of total RNA extracted. In *RAMP2*$^{+/-}$ mice, RAMP2 expression was about half that in WT mice, while AM expression was significantly upregulated. $n = 6$ per group. (**B–E**) Aortic ring assay. Representative photomicrographs of 7-day collagen gel cultures of aortas from 8-week-old mice (see Methods). Aortic explants from WT and *RAMP2*$^{+/-}$ mice were cultured in the absence or presence of VEGF (50 ng/ml), and capillaries sprouting from the edges of the rings were analyzed. The aortic explants from *RAMP2*$^{+/-}$ mice showed diminished angiogenesis. $n = 6$ per group. (**F** and **G**) Matrigel angiogenesis assay (see Methods). Representative photomicrographs showing angiogenesis in response to injected Matrigel. Capillary formation toward the Matrigel was greatly reduced in *RAMP2*$^{+/-}$ (**G**) compared with WT (**F**). $n = 6$ per group. (**H** and **I**) In vitro culture of AGM explant (see Methods). Representative photomicrographs showing the vascular network formation from the tissue cultured AGM region of E10.5 WT (**H**) and *RAMP2*$^{-/-}$ embryos (**I**). Vascular network formation was diminished in *RAMP2*$^{-/-}$ mice. $n = 4$ per group.

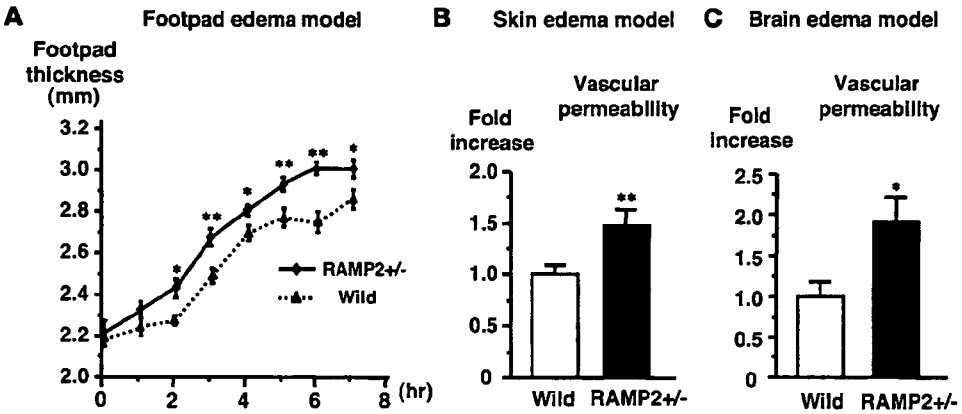

Figure 6

In vivo vascular permeability assay. (**A**) Footpad edema model. λ-Carrageenan was injected into the footpad of 8-week-old *RAMP2*$^{+/-}$ and WT mice to induce edema for the evaluation of vascular permeability in adult mice; swelling of the footpad was measured hourly using a thickness gauge. *RAMP2*$^{+/-}$ mice showed significantly greater swelling than WT mice. n = 12 per group. $^{**}P < 0.01$, $^{*}P < 0.05$ vs. WT. (**B**) Skin edema model (see Methods). Fluorescence intensity was measured using a fluorescence microplate reader. Permeability levels are presented relative to WT. *RAMP2*$^{+/-}$ mice (n = 8) showed significantly greater vascular permeability than WT mice (n = 13). $^{**}P < 0.01$ vs. WT. (**C**) Brain edema model (see Methods). Vascular permeability in *RAMP2*$^{+/-}$ mice (n = 12) is presented relative to that in WT mice (n = 10). *RAMP2*$^{+/-}$ mice showed significantly greater vascular permeability than WT mice. $^{*}P < 0.05$ vs. WT.

peutic angiogenesis, in that it increases vascular permeability and may exacerbate arteriosclerosis.

Studies of gene-targeted mice have led to the identification of angiogenic factors that had not previously been recognized for their angiogenic properties. AM was originally identified as a vasodilator, although it is now known to possess a variety of biological activities. Indicative of AM's novel angiogenic properties is our previous finding that *AM*$^{-/-}$ embryos die in utero due to hemorrhage and edema resulting from abnormalities of vascular development (14). We also showed previously that exogenous administration of AM enhances angiogenesis in ischemic tissues in adults, and therapeutic application of AM is much anticipated (25). Gene-targeted mice also provide information about the fundamental roles played by AM during the multistep process of angiogenesis. It is noteworthy, for instance, that *AM*$^{-/-}$ embryos die at a relatively late stage of development (E13.5–E14.5) compared with KO mice lacking other substances classified as angiogenic factors. This suggests that the vasculature does develop in *AM*$^{-/-}$ mice, but its fragile structure is likely disrupted after the start of circulation. It also clearly shows that AM is essential not only for angiogenesis, but also for vascular integrity.

As with other growth factors, the clinical applicability of AM has 2 serious limitations: AM is a peptide with a short half-life in the bloodstream, and the cost of the recombinant protein makes its use in the treatment of chronic diseases impractical. This prompted us to focus on AM's receptor system. McLatchie et al. showed that AM signaling is regulated by a unique control system (28). The main body of the AM receptor is thought to be CRLR, a 7-transmembrane domain GPCR. CRLR associates with 1 of 3 subtypes of RAMP, which determines the affinity of CRLR for its ligands. By generating RAMP2-specific KO mice, we have been able to demonstrate that RAMP2 is the key determinant of AM's function during vascular development. In our *RAMP2*$^{-/-}$ mice, CRLR and the other RAMPs were preserved; nevertheless, deletion of RAMP2 was sufficient to reproduce the phenotypes of the *AM*$^{-/-}$ genotype. Our finding that AM expression was upregulated in *RAMP2*$^{-/-}$ embryos just before their death further confirms that RAMP2 is essential for AM signaling during vascular development.

In both *AM*$^{-/-}$ and *RAMP2*$^{-/-}$ embryos, vascular fragility ultimately leads to hemorrhage and edema. Notably, however, the systemic edema was much more severe in *RAMP2*$^{-/-}$ mice. Edema was sometimes detected in *AM*$^{-/-}$ mice, but its severity varied. Moreover, administration of recombinant AM to crossbred *AM*$^{+/-}$ females increased the survival rate of *AM*$^{-/-}$ embryos at E14.5 (14), suggesting that maternally supplied AM partially compensates for the lack of embryonic AM expression. By contrast, *RAMP2*$^{-/-}$ mice cannot express a functional AM receptor in their vasculature and thus can not respond to maternal AM.

We found that neovascularization was diminished and vascular permeability was increased in adult *RAMP2*$^{+/-}$ mice, which showed reduced expression of RAMP2. We also found that *RAMP2*$^{+/-}$ mice had higher BP than did their WT littermates, which confirms that RAMP2 continues to be a crucial determinant of vascular function in the adult. Interestingly, we also found that the edema developed by *RAMP2*$^{+/-}$ mice in various disease models was more severe than that in WT mice, suggesting the AM-RAMP2 system could be an attractive therapeutic target for treating the edema often associated with vascular regenerative therapies, brain trauma, and infarction. In that regard, it is noteworthy that we were able to modulate the vascular function of AM by modulating RAMP2. Using RAMP2O/E cells, we clearly showed that by upregulating RAMP2 signaling, we could enhance capillary formation, firm up tight junctions, and reduce vascular permeability. RAMP2O/E cells were also resistant to apoptosis. Thus, RAMP2 could be a therapeutic target by which to manipulate the vascular functions of AM.

By contrast, RAMP3O/E cell lines did not show either enhanced angiogenesis or improved vascular stability, although RAMP3 has previously been shown to work with CRLR to function as another AM receptor (37). Furthermore, our finding that RAMP3 was expressed at WT levels in *RAMP2*$^{-/-}$ mice confirmed that RAMP3 cannot compensate for the absence of RAMP2 during vascular development. Consistent with the distinctly different physiologi-

cal roles played by RAMP2 and RAMP3, *RAMP3*$^{-/-}$ mice live apparently normally until old age (38). In addition, whereas RAMP2 and CRLR are downregulated in an endotoxemia model, RAMP3 is markedly upregulated (39), and it has been suggested that RAMP3 may be involved in post-endocytic receptor trafficking, as it presents a PDZ type I domain (40).

Signal transduction via GPCRs and the regulation of their function has long attracted the interest of many researchers. Indeed, about 40% of the drugs in clinical use today target GPCRs. We suggest that RAMP2 is an alternative therapeutic target by which to affect CRLR function. Because RAMP2 is a low-MW protein, structural analysis and the synthesis of specific agonists or antagonists are much more realistic for RAMP2 than for 7-transmembrane domain GPCRs, which has proven difficult. Moreover, because RAMP2 determines the vascular functions of AM, it would be expected that greater specificity would be achieved by targeting RAMP2 than by targeting CRLR, which can also function as a receptor for other ligands. In that context, our findings provide a clear basis for the development of drugs to modulate RAMP2 and, thereby, the vascular effects of AM.

Methods

Generation of RAMP2 KO mice. KO mice were generated as described previously (14, 16, 41, 42). Briefly, a plasmid-targeting vector was constructed to insert loxP sites encompassing exons 2–4 of *RAMP2* and the neomycin resistance gene, after which the plasmid was linearized and introduced into Bruce 4 embryonic stem cells by electroporation. Homologous recombinants were identified, and 2 independently targeted clones were injected into BALB/c blastocysts to generate chimeric mice. Male chimeras were crossbred with C57BL/6 females, and germline transmission was verified by Southern blot analysis. After obtaining heterozygotic floxed RAMP2 mice, we crossbred them with CAG-Cre mice to delete exons 2–4 of the *RAMP2* gene. The deletion of RAMP2 was certified by Southern blot analysis. The Cre gene was then removed from the line by backcrossing with C57BL/6 mice. All experiments were performed in accordance with the Declaration of Helsinki and were approved by the Shinshu University Ethics Committee for Animal Experiments.

In situ hybridization. In situ hybridization was performed as described previously (43). cRNAs were prepared from linearized cDNA templates of murine RAMP2 (ACACTTTGCGAACTGCTCCCTGGTGCAGCCCACCTTCTCTGATCCCCCAGAGGATGTGCTCCTGGCCATGATCATAGCCCCCATCTGCCTCATCCCGTTCCTTGTTACTCTTGTGGTGTGGAGGAGTAAAGACAGCGATGCCCAGGCCTAGGGTCCATTTCTCAGCAGCCATTTTTCCCCCCTTTTCCCTGCTGGAACCAGGAATGGCGCTCCTCCCCTCCCTACCCACTTACTCTCATCCTTCCCACAGACCTGTGGATTGGTGGAAATGGCAGCAAAGGGGACTCACGACACAATG) to generate antisense and sense probes. The cRNA transcripts were synthesized according to the manufacturer's instructions (Ambion).

Histological examination. Whole embryos, yolk sac and placenta, were fixed in 4% phosphate-buffered paraformaldehyde (pH 7.2), embedded in paraffin, and cut into 4-μm sections for histological examination. Some yolk sacs were used for immunohistochemical staining with anti-mouse CD31 antibody (BD Biosciences – Pharmingen) to visualize blood vessels. Samples were stained with a Histofine MOUSESTAIN KIT (Nichirei Biosciences) and DAB chromogen and counterstained with methyl green. Apoptosis was visualized in green fluorescence using the TUNEL method with an Apoptosis In Situ Detection Kit (Chemicon) and nuclei were stained with Hoechst 33342. To evaluate the aortic wall structure, immunohistochemical staining was performed using anti-mouse type IV collagen antibody (Collaborative Research), phalloidin, and DAPI (Roche Diagnostics). Confocal microscopic observation was then carried out using a Leica TCS-SP2 laser scanning microscope.

Transmission electron microscopy. Specimens were fixed in 2% glutaraldehyde (pH 7.2) and 4% osmium tetroxide, embedded in epoxy resin (Epok) 812 (Oken Shoji Co.), cut into ultrathin sections, double-stained with uranyl acetate and lead citrate, and examined by electron microscopy (JEM-1010; Jeol).

Quantitative real-time PCR analysis. Total RNA was extracted from tissues or cells using TRIzol Reagent (Invitrogen), after which it was treated with DNA-Free (Ambion) to remove contaminating DNA and subjected to reverse transcription using an Omniscript RT kit (QIAGEN) with random primers (Invitrogen). Quantitative real-time RT-PCR analysis was carried out using an ABI PRISM 7300 Sequence Detection System (Applied Biosystems) with SYBR Green (Toyobo) or TaqMan probe, and values were normalized to 18S rRNA (TaqMan Ribosomal RNA Control Reagents VIC Probe; Applied Biosystems). The primers and probes used were as follows: mouse AM (mAM) forward, 5′-CTACCGCCAGAGCATGAACC-3′; mAM reverse, 5′-GAAATGTGCAGGTCCCGAA-3′; mAM probe, 5′-CCCGCAGCAATGGATGCCG-3′; mRAMP2 forward, 5′-GCAGCCCACCTTCTCTGATC-3′; mRAMP2 reverse, 5′-AACGGGATGAGGCAGATGG-3′; mRAMP2 probe, 5′-CCCAGAGGATGTGCTCCTGGCCAT-3′; mRAMP3 forward, 5′-TGCAACGAGACAGGGATGC-3′; mRAMP3 reverse, 5′-GCATCATGTCAGCGAAGGC-3′; mRAMP3 probe, 5′-AGAGGCTGCCTCGCTGTGGGAA-3′; mCRLR forward, 5′-AGGCGTTTACCTGCACACACT-3′; mCRLR reverse, 5′-CAGGAAGCAGAGGAAACCCC-3′; mCRLR probe, 5′-ATCGTGGTGGCTGTGTTTGCGGAG-3′; mVE-cadherin forward: 5′-GGTGGCCAAAGACCCTGAC-3′; mVE-cadherin reverse, 5′-ACTGGTCTTGCGGATGGAGT-3′; mCDN5 forward, 5′-GCCTTCCTGGACCACAACA-3′; mCDN5 reverse, 5′-ACGACATCCACAGCCCCTT-3′; mCDN5 probe, 5′-CGTGACGGCGCAGACGACTTG-3′; mα2 type IV collagen forward, 5′-CACAACATCAACGATCCACCC-3′; mα2 type IV collagen reverse, 5′-GAACCCCATGATGCCTTCCT-3′; mα2 type IV collagen probe, 5′-AGCAAGGGATACCCGGCGTAATCTCA-3′; human VEGF (hVEGF) forward, 5′-TACCTCCACCATGCCAAGTG-3′; hVEGF reverse, 5′-GTGATGATTCTGCCCTCCTCC-3′; heNOS forward, 5′-AGATCTCCGCCTCGCTCAT-3′; heNOS reverse, 5′-AGCCATACAGGATTGTCGCC-3′; hCDN5 forward, 5′-AGGCGTGCTCTACCTGTTTTG-3′; hCDN5 reverse, 5′-AACTCGCGGACGACAATGTT-3′.

The PI3K inhibitor LY294002 (10^{-6} M) and a PKA inhibitor (14-22 cell permeable PKA inhibitor; 10^{-6} M) were obtained from Calbiochem.

Establishment of the RAMP2O/E line. The RAMP2O/E cell line was created using EAhy926 ECs, an immortal, clonally pure, human EC line obtained through hybridization of HUVECs and line A 549/8 lung carcinoma cells (kindly provided by C.J. Edgell, University of North Carolina, Chapel Hill, North Carolina, USA). EAhy926 human ECs were cultured in DMEM (Invitrogen) supplemented with 10% FBS (EQUITECH-BIO INC.). Full-length hRAMP2 cDNA was obtained from the UMR cDNA Resource Center (University of Missouri-Rolla). hRAMP2 (580 bp) labeled with HA-tag was inserted into the cloning site of pcDNA3.1$^+$ vector (Invitrogen), which was then linearized and transfected into EAhy926 cells using Effectene transfection reagent (QIAGEN). Four cell lines overexpressing RAMP2 were then cloned from G418-resistant (400 μg/ml) colonies. EAhy926 cells transfected with empty pcDNA3.1$^+$ vector served as controls.

Capillary formation on Matrigel. RAMP2O/E cells or control ECs were cultured on 24-well culture plates coated with Matrigel (BD) in medium containing 10^{-7} M recombinant hAM (Peptide Institute), and capillary formation was monitored microscopically. Photomicrographs were taken of 2 different fields in each well, and the degree of capillary formation was evaluated by quantification of the total capillary area in each field using

NIH Image software. Capillary area was then presented relative to the cell surface area of the control cells on day 1.

In vitro vascular permeability assay. To assay vascular permeability in vitro, we used a permeability chamber consisting of a 24-well tissue culture plate with cell culture inserts. The inserts contained a transparent polyethylene membrane with a high density of symmetrical pores (1 μm in diameter) that permitted high rates of basolateral diffusion. RAMP2O/E and control cells were seeded onto collagen-coated (Cellmatrix Type I-C; Nitta Gelatin Inc.) inserts, after which confluent endothelial monolayers that occluded the membrane pores were allowed to form over several days. The cell monolayers were then treated with 10 ng/ml VEGF, after which 13.3 mg/ml Dextran FITC Conjugate (MW 70,000; Research Organics) was added on top of the cells. The permeability of the monolayer was then assessed by measuring the fluorescence of the solution in the wells using a Multi-Detection Microplate Reader (POWERSCAN HT; DS Pharma Biomedical). The excitation and emission wavelengths were 485 nm and 530 nm, respectively.

Structure of tight junction after cell injury. EAhy926 ECs were cultured until confluent on chamber slides in DMEM containing 10^{-7} M AM and then exposed to 0.5 mM H_2O_2. Two hours after the H_2O_2 treatment, the cells were immunostained with anti-ZO-1 antibody (BD Biosciences – Pharmingen) and the nucleus-specific dye Hoechst 33342 (Sigma-Aldrich) and observed under a confocal microscope.

Aortic ring assay. After mice were killed with an overdose of anesthetic, the thoracic aorta was dissected from the posterior mediastinum, placed in serum-free EBM-2 endothelial basal medium (Cambrex), and cleaned of blood and fibroadipose tissue under a stereoscopic microscope using fine forceps and scissors. The vessel was then cut into 1-mm-long rings, which were subjected to 8 consecutive washes with serum-free EBM-2. The aortic rings were then embedded in thick collagen gel (Cellmatrix Type I-A; Nitta Gelatin Inc.) and cultured for 7 days, with or without recombinant hVEGF (50 ng/ml; R&D Systems) supplement. The capillaries that sprouted from the edges of the rings were analyzed (44).

Matrigel assay. After mice were anesthetized, 500 μl Matrigel (BD) containing 100 ng recombinant hbFGF (Wako) was injected subcutaneously into the dorsal region using a 25-gauge needle and permitted to solidify. Seven days later, the mice were killed with an overdose of anesthetic, the skin around the injected sites was incised, and the angiogenic response to the implanted Matrigel was analyzed.

AGM culture. Tissue culture of the AGM regions was carried out as described previously (45). The AGM regions were dissected from E10.5 embryos and plated on mouse OP9 stromal cells cultured on a 24-well dish. After 5 days of culture, capillaries growing from the AGM explant were stained with anti-CD31 antibody.

Footpad edema model. Vascular permeability leading to mouse footpad edema was assayed as described previously (46). Briefly, 20 μl of 0.01 g/ml λ-carrageenan (Wako) was injected subcutaneously into the footpads of 8-week-old mice, after which the swelling of the footpad was monitored using a thickness gauge (resolution, 1 μm).

Skin edema model. Vascular permeability leading to mouse skin edema was assayed as described previously (47). Mice were injected via the tail vein with 0.2 ml of 1.5% FITC-BSA (15 mg/ml) in isotonic Tyrode solution, which served as a tracer of vascular permeability. Thereafter, serum exudation was induced by subcutaneous injection of histamine (1 μg/100 μl/site) into the shaved dorsal skin. Thirty minutes later, the injected sites in the dorsal skin were removed as circular patches and put into the wells of a 24-well culture plate. Formamide (1 ml) was then added to each well and incubated at 50°C for 2 h, after which the fluorescence intensity in each well was measured using a Multi-Detection Microplate Reader; the excitation and emission wavelengths were 485 nm and 530 nm, respectively.

Brain edema model (cold lesion model). Mice were mounted in a stereotaxic frame (Narishige), after which the scalp was incised, subcutaneous tissue was retracted from the bone, and the skull was exposed. Using a drill, a circular craniotomy was then carried out over the right parietal cortex, extending from the lambda suture to bregma, and the resultant bone flap was lifted off to expose the underlying dura. The cold lesion was made using a copper cylinder (3 mm in diameter) that had been precooled with liquid nitrogen. The metal probe was lowered quickly onto the surface of the intact dura over the parietotemporal cortex under microscopic control and pressed down to a depth of 1 mm for 30 seconds (48).

To quantify the vascular permeability of brain vessels, 0.2 ml of sodium fluorescein at a concentration of 6 mg/ml in PBS was injected via the tail vein 24 hours after making the cold lesions. Thirty minutes later, the mice were anesthetized and perfused with PBS (20 ml) via the left cardiac ventricle to remove the fluorescent tracer from the vascular bed. To assess their fluorescence, brain hemispheres were homogenized in 0.5 M borate buffer (pH 10) and centrifuged (800 *g*) for 15 min at 4°C, after which the supernatant was added to 1.2 ml of ethanol to precipitate the proteins. The samples were again centrifuged, and the fluorescence in the supernatant was measured using a Multi-Detection Microplate Reader (49); the excitation and emission wavelengths were 330 nm and 485 nm, respectively.

Statistics. Quantitative values are expressed as mean ± SE. Student's *t* tests were used to determine significant differences. Values of $P < 0.05$ were considered significant.

Acknowledgments

We thank C.J. Edgell for EAhy926 cells. This study was supported by a grant from the Takeda Medical Research Foundation; a Japan Heart Foundation Research Grant; a Grant for Research on Cardiovascular Disease from the Tanabe Medical Conference; a grant from the Novartis Foundation for Gerontological Research; an Astra Zeneca Research Grant; grants from the Mitsui Life Social Welfare Foundation, the Ichiro Kanehara Foundation, the Uehara Memorial Foundation, the Sankyo Foundation of Life Science, the Naito Foundation, the Mitsubishi Pharma Research Foundation, and the Salt Science Research Foundation; Research Grant for Cardiovascular Disease 19C-7 from the Ministry of Heath, Labour and Welfare; and a Grant-in-Aid for Scientific Research from the Ministry of Education, Culture, Sports, Science and Technology, Japan.

Received for publication June 18, 2007, and accepted in revised form November 7, 2007.

Address correspondence to: Takayuki Shindo, Department of Organ Regeneration, Shinshu University Graduate School of Medicine, 3-1-1 Asahi, Matsumoto 390-8621, Japan. Phone: 81-263-37-3192; Fax: 81-263-37-3437; E-mail: t-shindo@sch.md.shinshu-u.ac.jp.

1. Kitamura, K., et al. 1993. Adrenomedullin: a novel hypotensive peptide isolated from human pheochromocytoma. *Biochem. Biophys. Res. Commun.* **192**:553–560.
2. Michibata, H., et al. 1998. Autocrine/paracrine role of adrenomedullin in cultured endothelial and mesangial cells. *Kidney Int.* **53**:979–985.
3. Kitamura, K., et al. 1994. Immunoreactive adrenomedullin in human plasma. *FEBS Lett.* **341**:288–290.
4. Jougasaki, M., et al. 1995. Renal localization and actions of adrenomedullin: a natriuretic peptide. *Am. J. Physiol.* **268**:F657–F663.
5. Nishikimi, T., and Matsuoka, H. 2005. Cardiac adrenomedullin: its role in cardiac hypertrophy and heart failure. *Curr. Med. Chem. Cardiovasc. Hematol. Agents.* **3**:231–242.
6. Samson, W.K., Murphy, T., and Schell, D.A. 1995. A novel vasoactive peptide, adrenomedullin, inhibits pituitary adrenocorticotropin release. *Endocrinology.* **136**:2349–2352.
7. Petrie, M.C., Hillier, C., Morton, J.J., and McMurray, J.J. 2000. Adrenomedullin selectively inhibits angiotensin II-induced aldosterone secretion in

humans. *J. Hypertens.* 18:61–64.
8. Isumi, Y., Kubo, A., Katafuchi, T., Kangawa, K., and Minamino, N. 1999. Adrenomedullin suppresses interleukin-1beta-induced tumor necrosis factor-alpha production in Swiss 3T3 cells. *FEBS Lett.* 463:110–114.
9. Shimosawa, T., et al. 2002. Adrenomedullin, an endogenous peptide, counteracts cardiovascular damage. *Circulation.* 105:106–111.
10. Shimosawa, T., et al. 2003. Deficiency of adrenomedullin induces insulin resistance by increasing oxidative stress. *Hypertension.* 41:1080–1085.
11. Kano, H., et al. 1996. Adrenomedullin as a novel antiproliferative factor of vascular smooth muscle cells. *J. Hypertens.* 14:209–213.
12. Miyashita, K., et al. 2003. Adrenomedullin promotes proliferation and migration of cultured endothelial cells. *Hypertens. Res.* 26(Suppl.):S93–S98.
13. Iwasaki, H., Eguchi, S., Shichiri, M., Marumo, F., and Hirata, Y. 1998. Adrenomedullin as a novel growth-promoting factor for cultured vascular smooth muscle cells: role of tyrosine kinase-mediated mitogen-activated protein kinase activation. *Endocrinology.* 139:3432–3441.
14. Shindo, T., et al. 2001. Vascular abnormalities and elevated blood pressure in mice lacking adrenomedullin gene. *Circulation.* 104:1964–1971.
15. Shindo, T., et al. 2000. Hypotension and resistance to lipopolysaccharide-induced shock in transgenic mice overexpressing adrenomedullin in their vasculature. *Circulation.* 101:2309–2316.
16. Oh-hashi, Y., et al. 2001. Elevated sympathetic nervous activity in mice deficient in alphaCGRP. *Circ. Res.* 89:983–990.
17. Niu, P., et al. 2004. Protective effects of endogenous adrenomedullin on cardiac hypertrophy, fibrosis, and renal damage. *Circulation.* 109:1789–1794.
18. Niu, P., et al. 2003. Accelerated cardiac hypertrophy and renal damage induced by angiotensin II in adrenomedullin knockout mice. *Hypertens. Res.* 26:731–736.
19. Nishimatsu, H., et al. 2002. Role of endogenous adrenomedullin in the regulation of vascular tone and ischemic renal injury: studies on transgenic/knockout mice of adrenomedullin gene. *Circ. Res.* 90:657–663.
20. Imai, Y., et al. 2002. Resistance to neointimal hyperplasia and fatty streak formation in mice with adrenomedullin overexpression. *Arterioscler. Thromb. Vasc. Biol.* 22:1310–1315.
21. Yamamoto, H., et al. 2007. Adrenomedullin insufficiency increases allergen-induced airway hyperresponsiveness in mice. *J. Appl. Physiol.* 102:2361–2368.
22. Kurihara, H., Shindo, T., Oh-Hashi, Y., Kurihar, Y., and Kuwaki, T. 2003. Targeted disruption of adrenomedullin and alphaCGRP genes reveals their distinct biological roles. *Hypertens. Res.* 26(Suppl.):S105–S108.
23. Nishimatsu, H., et al. 2003. Endothelial responses of the aorta from adrenomedullin transgenic mice and knockout mice. *Hypertens. Res.* 26(Suppl.):S79–S84.
24. Aoki-Nagase, T., et al. 2002. Attenuation of antigen-induced airway hyperresponsiveness in CGRP-deficient mice. *Am. J. Physiol. Lung Cell Mol. Physiol.* 283:L963–L970.
25. Iimuro, S., et al. 2004. Angiogenic effects of adrenomedullin in ischemia and tumor growth. *Circ. Res.* 95:415–423.
26. Fujii, T., et al. 2005. Adrenomedullin enhances therapeutic potency of bone marrow transplantation for myocardial infarction in rats. *Am. J. Physiol. Heart Circ. Physiol.* 288:H1444–H1450.
27. Nagaya, N., et al. 2005. Adrenomedullin: angiogenesis and gene therapy. *Am. J. Physiol. Regul. Integr. Comp. Physiol.* 288:R1432–R1437.
28. McLatchie, L.M., et al. 1998. RAMPs regulate the transport and ligand specificity of the calcitonin-receptor-like receptor. *Nature.* 393:333–339.
29. Kuwasako, K., Cao, Y.N., Nagoshi, Y., Kitamura, K., and Eto, T. 2004. Adrenomedullin receptors: pharmacological features and possible pathophysiological roles. *Peptides.* 25:2003–2012.
30. Parameswaran, N., and Spielman, W.S. 2006. RAMPs: The past, present and future. *Trends Biochem. Sci.* 31:631–638.
31. Morfis, M., Christopoulos, A., and Sexton, P.M. 2003. RAMPs: 5 years on, where to now? *Trends Pharmacol. Sci.* 24:596–601.
32. Montuenga, L.M., Martinez, A., Miller, M.J., Unsworth, E.J., and Cuttitta, F. 1997. Expression of adrenomedullin and its receptor during embryogenesis suggests autocrine or paracrine modes of action. *Endocrinology.* 138:440–451.
33. Montuenga, L.M., Mariano, J.M., Prentice, M.A., Cuttitta, F., and Jakowlew, S.B. 1998. Coordinate expression of transforming growth factor-beta1 and adrenomedullin in rodent embryogenesis. *Endocrinology.* 139:3946–3957.
34. Bauer, J., et al. 1992. In vitro model of angiogenesis using a human endothelium-derived permanent cell line: contributions of induced gene expression, G-proteins, and integrins. *J. Cell Physiol.* 153:437–449.
35. Edgell, C.J., Curiel, D.T., Hu, P.C., and Marr, H.S. 1998. Efficient gene transfer to human endothelial cells using DNA complexed to adenovirus particles. *Biotechniques.* 25:264–268, 270–272.
36. Lee, R.J., et al. 2000. VEGF gene delivery to myocardium: deleterious effects of unregulated expression. *Circulation.* 102:898–901.
37. Sexton, P.M., Albiston, A., Morfis, M., and Tilakaratne, N. 2001. Receptor activity modifying proteins. *Cell Signal.* 13:73–83.
38. Dackor, R.T., Fritz-Six, K.L., Smithies, O., and Caron, K.M. 2007. Receptor activity modifying proteins 2 and 3 have distinct physiological functions from embryogenesis to old age. *J. Biol. Chem.* 282:18094–18099.
39. Ono, Y., Okano, I., Kojima, M., Okada, K., and Kangawa, K. 2000. Decreased gene expression of adrenomedullin receptor in mouse lungs during sepsis. *Biochem. Biophys. Res. Commun.* 271:197–202.
40. Bomberger, J.M., Parameswaran, N., Hall, C.S., Aiyar, N., and Spielman, W.S. 2005. Novel function for receptor activity-modifying proteins (RAMPs) in post-endocytic receptor trafficking. *J. Biol. Chem.* 280:9297–9307.
41. Shindo, T., et al. 2000. ADAMTS-1: a metalloproteinase-disintegrin essential for normal growth, fertility, and organ morphology and function. *J. Clin. Invest.* 105:1345–1352.
42. Shindo, T., et al. 2002. Kruppel-like zinc-finger transcription factor KLF5/BTEB2 is a target for angiotensin II signaling and an essential regulator of cardiovascular remodeling. *Nat. Med.* 8:856–863.
43. Lyons, G.E., Schiaffino, S., Sassoon, D., Barton, P., and Buckingham, M. 1990. Developmental regulation of myosin gene expression in mouse cardiac muscle. *J. Cell Biol.* 111:2427–2436.
44. Zhu, W.H., Iurlaro, M., MacIntyre, A., Fogel, E., and Nicosia, R.F. 2003. The mouse aorta model: influence of genetic background and aging on bFGF- and VEGF-induced angiogenic sprouting. *Angiogenesis.* 6:193–199.
45. Hamaguchi, I., et al. 1999. In vitro hematopoietic and endothelial cell development from cells expressing TEK receptor in murine aorta-gonad-mesonephros region. *Blood.* 93:1549–1556.
46. Sakurai, K., et al. 1997. Anti-inflammatory activity of superoxide dismutase conjugated with sodium hyaluronate. *Glycoconj. J.* 14:723–728.
47. Yamaki, K., Takano-Ishikawa, Y., Goto, M., Kobori, M., and Tsushida, T. 2002. An improved method for measuring vascular permeability in rat and mouse skin. *J. Pharmacol. Toxicol. Methods.* 48:81–86.
48. Hortobagyi, T., et al. 2000. A novel brain trauma model in the mouse: effects of dexamethasone treatment. *Pflugers Arch.* 441:409–415.
49. Schoch, H.J., Fischer, S., and Marti, H.H. 2002. Hypoxia-induced vascular endothelial growth factor expression causes vascular leakage in the brain. *Brain.* 125:2549–2557.

ELSEVIER

Bone 36 (2005) 1056 – 1064

BONE

www.elsevier.com/locate/bone

Complementary antagonistic actions between C-type natriuretic peptide and the MAPK pathway through FGFR-3 in ATDC5 cells

Ami Ozasa[a], Yasato Komatsu[a,*], Akihiro Yasoda[a], Masako Miura[a], Yoko Sakuma[a], Yuko Nakatsuru[a], Hiroshi Arai[a], Nobuyuki Itoh[b], Kazuwa Nakao[a]

[a]*Department of Medicine and Clinical Science, Kyoto University Graduate School of Medicine, 54 Shogoin Kawahara-cho Sakyo-ku, Kyoto 606-8507, Japan*
[b]*Department of Genetic Biochemistry, Kyoto University Graduate School of Pharmaceutical Sciences, Japan*

Received 30 September 2004; revised 10 February 2005; accepted 7 March 2005

Abstract

We previously reported that C-type natriuretic peptide (CNP) stimulates endochondral ossification and corrects the reduction in body length of achondroplasia model mouse with constitutive active fibroblast growth factor receptor 3 (FGFR-3). In order to examine the interaction between CNP and FGFR-3, we studied intracellular signaling by using ATDC5 cells, a mouse chondrogenic cell line, and found that FGF2 and FGF18 markedly reduced CNP-dependent intracellular cGMP production, and that these effects were attenuated by MAPK inhibitors. Western blot analysis demonstrated that the level of GC-B, a particulate guanylyl cyclase specific for CNP, was not changed by treatment with FGFs. Conversely, CNP and 8-bromo-cGMP strongly and dose-dependently inhibited the induction of ERK phosphorylation by FGF2 and FGF18 without changing the level of FGFR-3, although they did not affect the phosphorylation of STAT-1. In the organ-cultured fetal mouse tibias, CNP and FGF18 counteracted on the longitudinal bone growth, and both the size and number of hypertrophic chondrocytes. The FGF/FGFR-3 pathway is known as the negative regulator of endochondral ossification. We found that FGFs inhibited CNP-stimulated cGMP production by disrupting the signaling pathway through GC-B while CNP antagonized the activation of the MAPK cascade by FGFs. These results suggest that the CNP/GC-B pathway plays an important role in growth plate chondrocytes and constitutes the negative cross talk between FGFs and the activity of MAPK. Our results may explain one of the molecular mechanisms of the growth stimulating action of CNP and suggest that activation of the CNP/GC-B pathway may be effective as a novel therapeutic strategy for achondroplasia.

Keywords: Natriuretic peptide; Guanylyl cyclase; Chondrocyte; FGF; MAPK

Introduction

The natriuretic peptide family consists of three structurally related peptides: atrial natriuretic peptide (ANP), brain natriuretic peptide (BNP) and C-type natriuretic peptide (CNP) [1]. They can influence a variety of homeostatic processes by accumulation of the intracellular guanosine 3′, 5′-cyclic monophosphate (cGMP) through two subtypes of particulate guanylyl cyclase (GC), GC-A for ANP and BNP, and GC-B for CNP [2]. In skeletal tissues, we have demonstrated that CNP is a positive growth regulator of long bones formed through endochondral ossification via the GC-B/cGMP pathway [3,4]. CNP-depleted mice are characterized by short stature with a phenotype histologically similar that of achondroplasia [3], while the growth plates of explanted long bones in the presence of CNP show a similar histological picture to that of the growth plate cartilage of fibroblast growth factor receptor 3 (FGFR-3)-depleted mice [5]. This raises the possibility that activation of the CNP/GC-B pathway of endochondral bone regulation reverses the inhibitory effect of FGFR-3 signaling in skeletogenesis.

FGFR-3 belongs to a class of tyrosine kinase receptors involved in signal transduction. In the presence of soluble or

* Corresponding author. Fax: +81 75 771 9452.
E-mail address: komatsuy@barium.rirc.kyoto-u.ac.jp (Y. Komatsu).

8756-3282/$ - see front matter © 2005 Elsevier Inc. All rights reserved.
doi:10.1016/j.bone.2005.03.006

cell-surface heparin sulfate proteoglycans, fibroblast growth factors (FGFs) binding to FGFRs induce receptor dimerization and autophosphorylation on tyrosine residues. This then triggers cell proliferation or differentiation through the Ras-Raf-dependent and phospholipase C-dependent signal transduction pathways involving MAPK stimulation [6]. FGFR-3 mutations have been shown to be responsible for achondroplasia, hypochondroplasia and thanatophoric dysphasia (TDI and TDII) [7,8]. These mutations activate receptor signaling by either inducing ligand-independent receptor dimerization or easing the constraints on autophosphorylation of receptor-tyrosine kinase [9]. It has recently been reported that, of the 23 members of the FGF family, FGF-18 is a physiologic ligand for FGFR-3 in chondrocytes and plays an important role as a mediator in skeletal development [10–12].

To gain further insight into the cellular basis of the interaction between CNP and FGFs in endochondral bone formation, we used ATDC5 cells, which constitute a mouse chondrogenic cell line derived from embryogenic carcinoma cells [13]. In the presence of insulin, these cells differentiate into chondrocytes, form cartilage nodules, serially exhibit several differentiation markers for the chondrocytes, and are eventually mineralized, thus reflecting the endochondral ossification process in vivo. We previously demonstrated that ATDC5 cells contain particularly high activity levels for GC-B and also appear to contain low levels of GC-A and the soluble form of guanylyl cyclase, which is responsive to nitric oxide [14]. Therefore, ATDC5 cells are considered to be a good model to study the interaction between CNP and FGFs in vitro.

We also studied the effects of CNP and FGF18 on organ-cultured fetal mouse tibias. Since the growth plates consist of several zones, each representing a different stage of differentiation and functioning differently, the interaction between the cells in the different zones can be crucial for a given substance to exert its effects. We previously developed an ex vivo organ culture system of mouse long bones [4]. During a 5-day culture, the bones exhibited longitudinal growth mostly due to the growth in the cartilage primordial rather than the ossified portion. This system was therefore considered a good ex vivo model for studying the interaction between CNP and FGFs. The purpose of the study presented here was to clarify the interaction between the CNP/GC-B pathway and FGF signaling in growth plate chondrocytes, as well as the mechanism of this interaction, in order to determine the efficacy of activation of CNP/GC-B as a novel therapeutic strategy for achondroplasia.

Materials and methods

Human C-type natriuretic peptide was purchased from Peptide Institute, Inc. (Minoh, Japan), 8-bromo cGMP and isobutylmethylxanthine (IBMX) from Sigma-Aldrich Co. (St. Louis, MO, USA), and human recombinant FGF2 from Pepro Tech EC. Ltd. (London, England). Rat recombinant FGF18 was generously provided by Amgen Inc. (Thousand Oaks, CA, USA). Primary antibodies, rabbit anti-phospho-ERK1/2 antibodies, rabbit anti- ERK1/2 antibodies, and anti-STAT-1 antibodies were obtained from Cell Signaling Technology Inc. (Beverly, MA, USA), rabbit anti-phospho-STAT-1 antibodies from Upstate Biotechnology, (Lake Placid, NY, USA), and HRP-conjugated donkey anti-rabbit IgG antibodies from Amersham Pharmacia Biotech, (Freiburg, Germany). The MEK (MAPK-ERK kinase) inhibitors U0126 and PD098059 were purchased from Cell Signaling Technology Inc., fetal calf serum (FCS) was purchased from Sankou Junyaku (Tokyo, Japan), and Ham F12/DMEM 50/50 medium and Bigger's BJG medium were obtained from GIBCO (Grand Island, NY, USA).

Cell culture conditions

Cells were grown and maintained using standard techniques. ATDC5 cells were maintained in Ham F12/DMEM 50/50 medium containing 5% FCS, antibiotics, and insulin (10 ng/ml). Confluent cells were maintained for 14 days and considered quiescent after maintenance in 0.5% FCS for 24 h. For radioimmunoassay, cells were seeded on 24-multiwell culture plates, and on a 6 cm dish (BD Bioscience, NJ, USA) for Western blotting and real-time PCR analysis.

Intracellular cGMP determination

Quiescent cells were treated with FGFs for 1 h. The cells were then preincubated in Ham F12/DMEM 50/50 medium containing 0.5% FCS and 1 mM IBMX at room temperature for 10 min. CNP was added at a concentration of 10^{-9}–10^{-7} M and incubated at 37°C for 30 min in the presence of 1 mM IBMX. Reactions were terminated immediately by aspirating the medium, washing the cells with ice-cold PBS, and freezing them in 500 μl of 50 mM HCl. The acidified extracts were analyzed for guanylyl cyclase activity. The level of cGMP was determined by radioimmunoassay after succinylation (Yamasa Co. Ltd., Chosi, Chiba, Japan). To examine the effect of FGFs, we also used the MEK inhibitors U0126 and PD098059, which were added 1 h before treatment of CNP. The level of cGMP was determined as already described.

Western blot analysis

Quiescent cells were incubated with a medium containing CNP (10^{-7}–10^{-6} M) or 10^{-4} M 8-bromo cGMP for 1 h. The medium was then switched to an FGF-containing one, and the cells were treated with FGFs (10 ng/ml) for 3 min. Cells were extracted with the aid of a solvent solution (0.5 M Tris–HCl, 10% SDS, β-mercaptoethanol, glycerol, and Bromo-phenol blue). Soluble proteins were electrophoretically resolved on 8% acrylamide, 0.1% SDS gels and

transferred to polyvinylidene fluoride membranes (Immobilon-P; Millipore, Billerica, MA, USA). The membranes were probed overnight with antibodies against phosphorylated ERK1/2, ERK1/2, phosphorylated STAT-1 or STAT-1, according to the supplier's instructions. The membranes were then probed with secondary antibodies for 1 h. Bound antibodies were detected by chemiluminescence (ECL, Amersham Pharmacia Biotech, Piscataway, NJ, USA) and their density measured by using the public domain National Institute of Health IMAGE program.

The expression of GC-B in ATDC5 cells was analyzed by Western blot analysis. Quiescent cells were incubated with a medium containing FGF18 (1 or 10 ng/ml) for 1 h, after which the cells were extracted and the proteins blotted to the membrane as described above. The membranes were probed for 1 h with the rabbit polyclonal anti-GC-B antibody [15] (a generous gift from Dr. D.L. Garbers of the University of Texas Southwestern Medical Center) and bound antibodies were detected as described above.

To confirm the effect of the MEK inhibitor on phosphorylated ERK1/2, we used 20 μM U0126, and the MEK inhibitor (U0126) was added 1 h before treatment of FGF2.

Real-time PCR analysis of FGFR-3

Quiescent cells were incubated with a medium containing CNP (10^{-6} M) for 1 h and total RNAs were extracted using ISOGEN (Nippon Gene Co. Ltd., Toyama, Japan) according to the manufacturer's instructions. After synthesis of the first-strand cDNA from 1 μg of total RNA by means of Superscript II RT (Life Technologies, Inc., St. Louis, MO, USA) with random hexamers, Taqman-PCR was performed with the ABI Prism 7700 sequence detection system and Taqman Universal PCR Mastermix (Applied Biosystems, Foster City, CA, USA) using FAM and VIC-labeled fluorogenic probes specific for FGFR-3 or the internal standard 18 S rRNA. All samples were run in duplicate in 96-well plates in the ABI Prism 7700 sequence. There was no significant difference in 18 S rRNA levels among experimental groups.

Organ culture of embryonic mouse tibias

Organ culture of fetal mouse tibias was performed with the suspension culture technique in a chemically defined medium (Bigger's BJG medium). Tibial explants from 16-day-old normal ICR mouse embryos were cultured for 5 days with or without 10 ng/ml FGF18 and 10^{-7} M CNP. After a 5-day culture, the total bone length was measured longitudinally by using a linear ocular scale mounted on an inverted microscope. Explants were fixed in 4% paraformaldehyde, decalcified in 10% EDTA/0.1 M Tris–HCl, pH 7.4, for 7 days, and embedded in paraffin. 5-μm-thick sections cut from the paraffin-embedded specimens were stained with Alcian blue (pH 2.5) and hematoxylin/eosin (H&E).

Immunohistochemical staining for type X collagen, using a polyclonal rabbit anti-type X collagen antibody (1:5000; LSL, Tokyo, Japan) as a primary antibody, was also performed. Immunoreactions were visualized by using a biotinylated antipolyvalent antibody, a streptavidin–biotin–horseradish peroxidase complex, and diaminobenzidine (Vector Laboratories, Inc., Burlingame, CA, USA). The specificity of the immunoreactions was controlled by omitting the primary antibody.

The size of hypertrophic cells was measured on 5-μm-thick sections of cultured tibias with a computerized measurement system (KS400 Imaging System; Carl Zeiss, Eching, Germany), and the cells of hypertrophic chondrocytes were manually counted.

Statistical analysis

Data are expressed as the mean ± SE. The changes in cGMP were compared by means of ANOVA using Fisher's test. Comparisons between groups of organ cultured bone lengths were performed with the unpaired *t* test. Probabilities less than 0.05 were considered statistically significant.

Results

Inhibition by FGF2 of CNP signaling in ATDC5 cells

ATDC5 cells were differentiated into chondrocytes for a 14-day culture after confluency [13], and we confirmed that collagen type X, a marker of hypertrophic chondrocytes, was expressed in these cells [16]. In ATDC5 cells, CNP (10^{-9}–10^{-7} M) stimulated the production of intracellular cGMP in a dose-dependent manner with a 36-fold increase of the basal level at 10^{-7} M CNP (55 ± 3 fmol/well to 1985 ± 181 fmol/well). This increase was inhibited up to 53% by the addition of 10 ng/ml of FGF2 (1045 ± 65 fmol/well) (Fig. 1A). Pretreatment with U0126, a specific inhibitor of the upstream of ERK (MEK) [17], at a concentration of 20 μM partially undid the reduction of cGMP by FGF2 (1395 ± 144 fmol/well vs. 1980 ± 143 fmol/well) compared with the vehicle (Fig. 1B). The same level of recovery was observed after pretreatment with another MEK inhibitor, PD098059, also at a concentration of 20 μM (1425 ± 276 fmol/well vs. 1620 ± 206 fmol/well). Western blot analysis was performed to confirm the blockade of U0126 to ERK1/2 phosphorylation by FGF2. Pretreatment with 20 μM U0126 completely blocked the phosphorylation of ERK1/2 (Fig. 1B inset).

Inhibition by FGF18 of CNP signaling in ATDC5 cells

We analyzed the effect of FGF18, the specific ligand for FGFR-3 in chondrocytes, on CNP-dependent cGMP production in ATDC5 cells. As in the case of FGF2, FGF18 inhibited intracellular cGMP production in ATDC5 cells in a dose-dependent manner (0.3–100 ng/ml). Preincubation

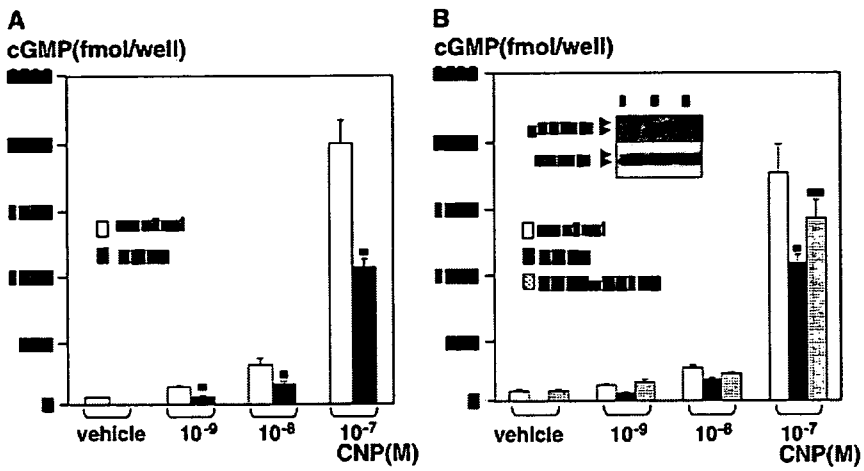

Fig. 1. Inhibition by FGF2 of CNP signaling in ATDC5 cells. The effects of FGF2 on CNP-dependent cGMP production in ATDC5 cells. (A) Controls (open columns) show CNP stimulation of the intracellular cGMP production in a dose-dependent manner (10^{-9}–10^{-7} M CNP), and this increase was inhibited by pretreatment with 10 ng/ml FGF2 (closed columns). Columns represent means ± SE (n = 6, each), *P < 0.01 vs. control (B) MEK inhibitor, U0126 (dotted columns) resulted in recovery from the reduction of cGMP by 10 ng/ml FGF2 (closed columns). Columns represent means ± SE (n = 6, each), *P < 0.01 vs. control (DMSO 0.0025%) (open columns), **P < 0.01 vs. FGF2. Inset, 20 μM U0126 completely blocked the phosphorylation of ERK1/2 in ATDC5 cells. 1: Control (DMSO 0.0025%), 2: treatment with 10 ng/ml FGF2, 3: pretreatment with 20 μM U0126.

with 3 ng/ml FGF18 significantly inhibited the increase in 10^{-7} M CNP stimulated cGMP production (1425 ± 82 fmol/well vs. 1975 ± 111 fmol/well). This inhibition by FGF18 reached 64% at a concentration of 10 ng/ml and 100 ng/ml FGF18 (1255 ± 11 fmol/well) (Fig. 2).

No effect of FGF18 on GC-B expression in ATDC5 cells

To confirm the expression level of GC-B, the specific receptor for CNP in ATDC5 cells, we performed Western blot analysis using antiserum specific for GC-B. The quiescent ATDC5 cells expressed a certain amount of GC-B at 120-kDa band, which incubation with FGF18 (1 or 10 ng/ml) for 1 h did not alter (Fig. 2 inset).

Attenuation by CNP of MAPK activity of FGFs

The effect of CNP on the downstream signaling of FGFR-3 in ATDC5 cells was analyzed next. ERK1/2 phosphorylation was barely detectable at the basal level but was noticeably stimulated with the addition of FGF2 (10 ng/ml) and FGF18 (10 ng/ml) in ATDC5 cells. Treatment of quiescent ATDC5 cells with CNP (10^{-7}–10^{-6} M) for 1 h prior to the addition of FGF2 and FGF18 reduced the phosphorylation of ERK1/2 in a dose-dependent manner. 10^{-6} M CNP completely eliminated the FGF-stimulated phosphorylation of ERK1/2 (Figs. 3A, B), while 10^{-4} M 8-bromo cGMP also inhibited ERK1/2 phosphorylation of FGF2 (Fig. 3C).

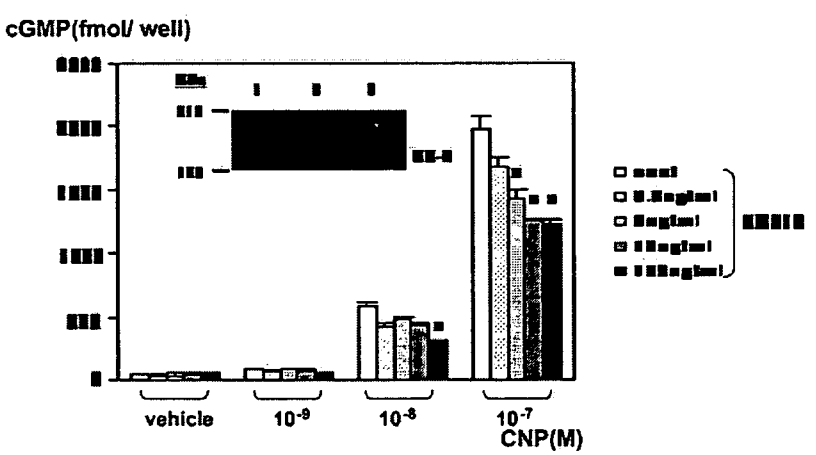

Fig. 2. Inhibition by FGF18 of CNP signaling in ATDC5 cells. The effects of FGF18 on CNP-dependent cGMP production in ATDC5 cells. As in the case of FGF2, FGF18 inhibited the increase in CNP induced cGMP in a dose-dependent manner (0.3–100 ng/ml). Columns represent means ± SE (n = 6, each), *P < 0.01 vs. control. Inset, expression of GC-B in ATDC5 cells (Western blot analysis). 1: Vehicle, 2: treatment with 1 ng/ml FGF18, 3: treatment with 10 ng/ml FGF18.

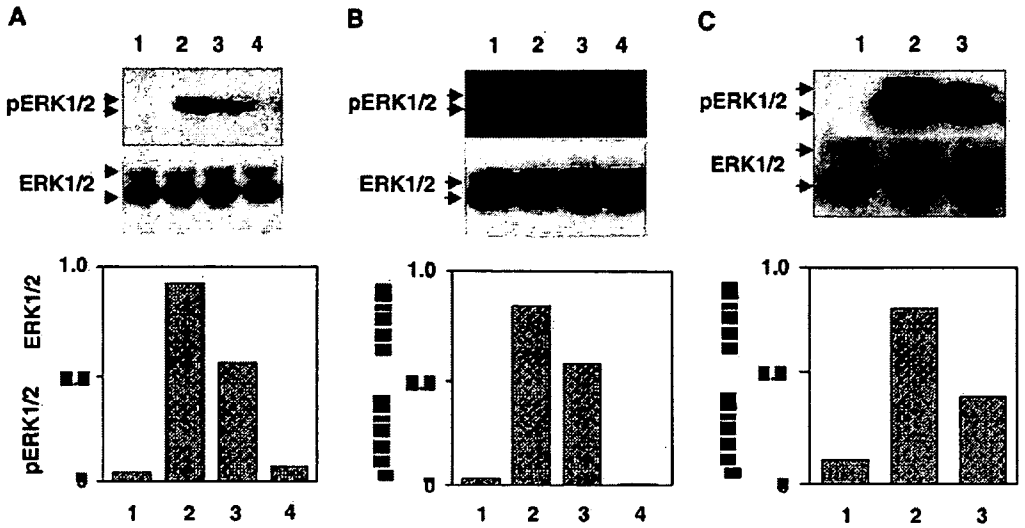

Fig. 3. Attenuation by CNP of MAPK activity of FGFs. CNP and cGMP reduced FGF-stimulated elevation of phosphorylated ERK1/2. ATDC5 cell extracts were examined with Western blotting for phosphorylated ERK1/2 (pERK1/2) and total ERK1/2 (ERK1/2) as described under Materials and methods. (A) CNP diminished FGF2-stimulated elevation of phosphorylated ERK1/2. 1: Vehicle, 2, 3, 4: stimulation with 10 ng/ml FGF2, 3: preincubation with 10^{-7} M CNP, 4: preincubation with 10^{-6} M CNP. (B) CNP attenuated FGF18-stimulated elevation of phosphorylated ERK1/2. 1: Vehicle, 2, 3, 4: stimulation with 10 ng/ml FGF18, 3: preincubation with 10^{-7} M CNP, 4: preincubation with 10^{-6} M CNP. (C) 8-bromo cGMP decreased FGF2-stimulated elevation of phosphorylated ERK1/2. 1: Vehicle, 2, 3: stimulation with 10 ng/ml FGF2, 3: preincubation with 10^{-4} M 8-Bromo cGMP. Representative blots are shown, and the relative levels of proteins were measured as phospho-ERK1/2/ERK1/2 density values. Each experiment was repeated 3 times, and data from a representative experiment are shown.

No change in STAT-1 phosphorylation in ATDC5 cells by FGFs or CNP

STAT-1 phosphorylation was already detectable at the basal level in ATDC5 cells. The level of phosphorylated STAT-1 remained unchanged when treated with FGF2 or FGF18 for 3, 10, 15, 30, or 60 min. Treatment of quiescent ATDC5 cells with CNP (10^{-7}–10^{-6} M) prior to the addition of FGF2 (10 ng/ml) and FGF18 (10 ng/ml) did not alter the amount of phosphorylated STAT-1 (Figs. 4A,

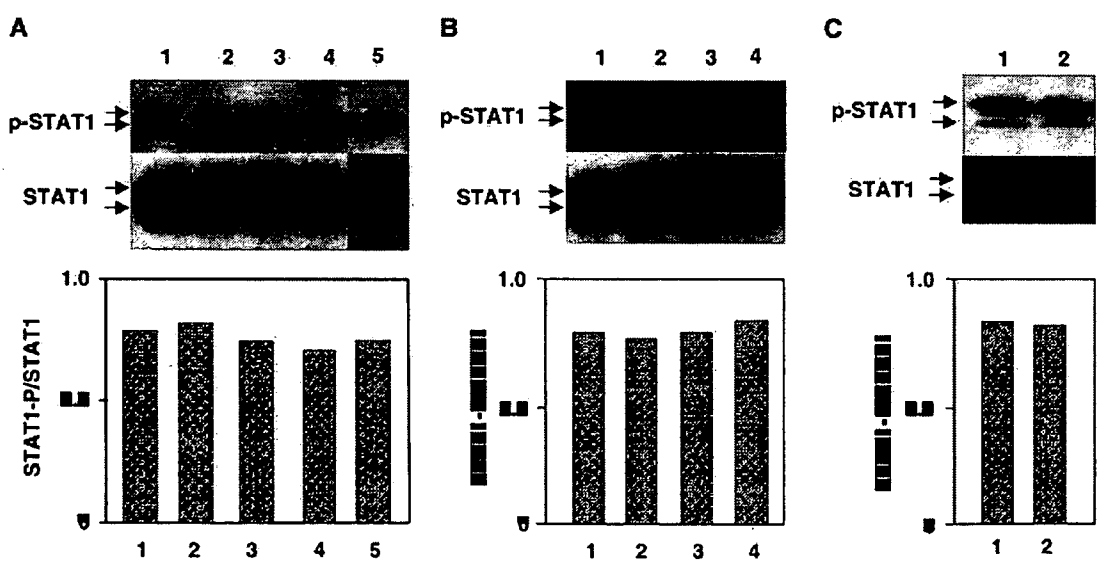

Fig. 4. No change in STAT-1 phosphorylation in ATDC5 cells by FGFs or CNP. Effects of CNP on the STAT-1 pathways of FGFs. ATDC5 cell extracts were examined with Western blotting for phosphorylated STAT-1 (pSTAT-1) and total STAT-1 (STAT-1) as described under Materials and methods. (A) CNP and 8-bromo cGMP did not alter the level of phosphorylated STAT-1 after FGF2 stimulation. 1: Vehicle, 2, 3, 4, 5: stimulation with 10 ng/ml FGF2, 3: preincubation with 10^{-7} M CNP, 4: preincubation with 10^{-6} M CNP, 5: preincubation with 10^{-4} M 8-bromo cGMP. (B) CNP did not alter the level of phosphorylated STAT-1 after FGF18 stimulation. 1: Vehicle, 2 3, 4: stimulation with 10 ng/ml FGF18, 3: preincubation with 10^{-7} M CNP, 4: preincubation with 10^{-6} M CNP. (C) CNP did not alter the basal expression of phosphorylated STAT-1. 1: Vehicle, 2: 10^{-6} M CNP alone. Representative blots are shown, and the relative levels of proteins were measured as the phospho-STAT-1/STAT-1 density values. Each experiment was repeated 3 times, and the data from a representative experiment are shown.

B), nor did CNP itself (10^{-6} M) affect the basal level of phosphorylated STAT-1 in ATDC5 cells (Fig. 4C), or treatment of quiescent ATDC5 cells with 10^{-4} M 8-bromo cGMP prior to the addition of FGF2 (10 ng/ml) cause no change in the amount of phosphorylated STAT-1 (Fig. 4A).

No effect of CNP on FGFR-3 expression in ATDC5 cells

FGFR3 mRNA levels in ATDC5 cells treated with the vehicle and pretreated with CNP (10^{-6} M) were 1.00 ± 0.06 and 1.04 ± 0.12 in arbitrary units, respectively, and this difference was not significant.

Effect of CNP and FGF18 on mouse fetal tibia organ culture

The organ culture of fetal mouse tibias provides a unique in vitro experimental model system of endochondral ossification. For our study, we used cultured tibias prepared from ICR mice, to examine the effects of CNP and FGF18. Treatment with 10^{-7} M CNP for 5 days produced a 12% increase in the total length of tibial explants compared with vehicle-treated explants (vehicle treated: 3.56 ± 0.05 mm vs. CNP treated: 3.99 ± 0.07 mm). On the other hand, treatment with 10 ng/ml FGF18 for 5 days resulted in a 6% decrease in the total length of tibial explants compared with vehicle-treated explants (vehicle treated: 3.57 ± 0.03 mm vs. FGF18 treated: 3.37 ± 0.04 mm). Treatment with a combination of 10^{-7} M CNP and 10 ng/ml FGF18 increased the total length of tibial explants for 8% compared with vehicle-treated explants (vehicle treated: 3.55 ± 0.04 mm vs. CNP and FGF18 treated: 3.84 ± 0.06 mm). These differences were all statistically significant ($P < 0.01$) (Fig. 5).

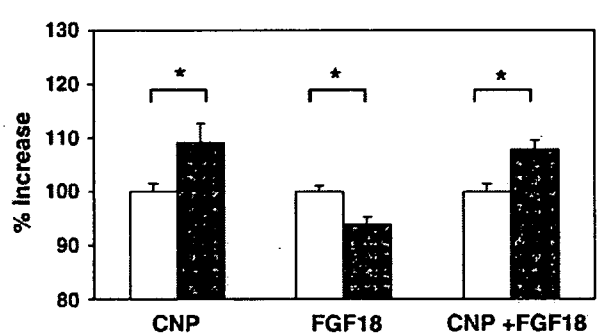

Fig. 5. Effect of CNP and FGF18 on mouse fetal tibia organ culture. Percent change in total length of fetal mouse tibias cultured with CNP and/or FGF18 for 5 days. Open columns show the percent change in total length of one tibia from mouse fetus treated with the vehicle. Hatched columns show the percent change in total length of the other tibia from the same mouse treated with 10^{-7} M CNP, 10 ng/ml FGF18, or with a combination of 10^{-7} M CNP and 10 ng/ml FGF18. Columns represent means ± SE ($n = 5$, each), *$P < 0.01$ vs. vehicle.

Effect of CNP and FGF18 on cell size and cell numbers of the growth plate chondrocytes

Microscopic examination disclosed elongation of the growth plate in mouse tibias cultured with 10^{-7} M CNP. Higher magnification of Alcian blue HE staining (Figs. 6A, B, E, F) and immunohistochemical staining for type X collagen (Figs. 6I, J) showed that the hypertrophic chondrocyte layer increased after treatment with 10^{-7} M CNP compared with treatment with the vehicle. The mean size of hypertrophic chondrocytes was markedly increased (vehicle treated: 497.85 ± 19.2 vs. CNP treated: 1071.42 ± 53.5 μm^2) (Fig. 7A), and the number of cells in the hypertrophic chondrocyte layer was reduced (vehicle treated: 152.67 ± 4.1 vs. CNP treated: 118 ± 3.61 cells) (Fig. 7B). In contrast, culturing with 10 ng/ml FGF18 caused shortening of the growth plate in cultured mouse tibias compared with that in vehicle-treated ones. Higher magnification of Alcian blue HE staining (Figs. 6A, C, E, G) and immunohistochemical staining for type X collagen (Figs. 6I, K) demonstrated that the hypertrophic chondrocyte layer was reduced. Not only the cell size (vehicle treated: 497.85 ± 19.2 vs. FGF18 treated: 314.01 ± 23.67 μm^2) (Fig. 7A), but also the number of hypertrophic chondrocytes was reduced by the treatment with 10 ng/ml FGF18 (vehicle treated: 152.67 ± 4.1 vs. FGF18 treated: 89.3 ± 1.45 cells) (Fig. 7B). Culturing with both 10^{-7} M CNP and 10 ng/ml FGF18 resulted in recovery by CNP of shortening of the growth plate in cultured mouse tibias by FGF18. Higher magnification of Alcian blue HE staining (Figs. 6C, D, G, H) and immunohistochemical staining for type X collagen (Figs. 6K, L) showed an increase in the hypertrophic chondrocyte layer compared with that of the FGF18-treated ones. The mean size of hypertrophic chondrocytes also increased compared with that of FGF18-treated ones (FGF18 treated: 314.01 ± 23.67 vs. CNP and FGF18 treated: 751.16 ± 41.6 μm^2) (Fig. 7A), and the reduction in number was also undone by CNP (FGF18 treated: 89.3 ± 1.45 vs. CNP and FGF18 treated: 145.3 ± 4.41 cells) (Fig. 7B).

Discussion

The study reported here used two different experimental designs to examine the interaction of the CNP/GC-B and FGFR-3 pathways in mouse chondrogenic ATDC5 cells and in organ-cultured tibias. In this study we were able to show that: (1) ATDC5 cells express GC-B, (2) FGF2 and FGF18 reduce CNP-dependent cGMP production in a dose-dependent manner without changing the amount of GC-B, (3) MAPK inhibitors attenuate the FGF inhibition of CNP-dependent cGMP production, (4) both CNP and cGMP inhibit the MAPK pathway but not the STAT-1 pathway of FGFR-3 activation without changing the amount of FGFR-3, and (5) CNP and FGF18 counteract longitudinal bone growth in organ cultured tibias.

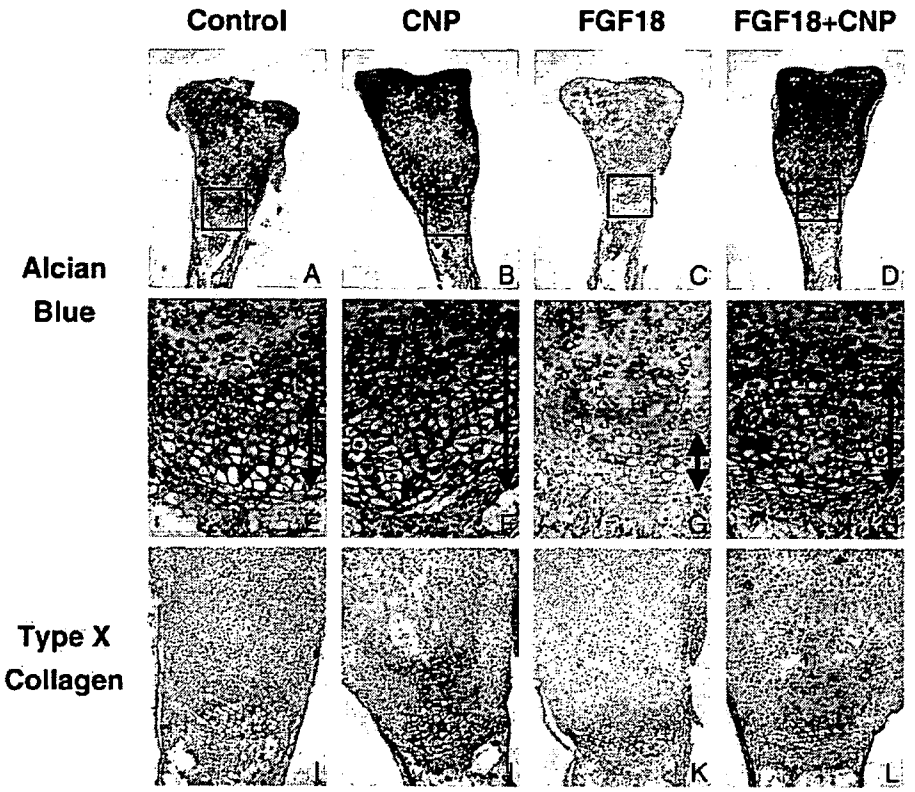

Fig. 6. Effect of CNP and FGF18 on mouse fetal tibia organ culture. Alcian blue and hematoxylin–eosin staining (upper and middle panels), and immunohistochemical staining for type X collagen (bottom panel) of cultured tibiae with CNP and/or FGF18. A, E, I: control; B, F, J: 10^{-7} M CNP; C, G, K: 10 ng/ml FGF18; D, H, L: 10 ng/ml FGF18 and 10^{-7} M CNP. Arrows indicate the hypertrophic chondrocyte zone. (A–D: magnification ×4, E–H: magnification ×20, I–L: magnification ×10.)

Substantial evidence exists that CNP is an antagonist of mitogenic action in many cell types. Activation of the CNP/GC-B pathway in the vascular smooth muscle cells was found to attenuate the onset of DNA synthesis, diminish cell proliferation, and inhibit chemotaxis [18]. As for the interaction of CNP with FGF signaling, marked elevation of cGMP induced by CNP had been reported to block the activation of the MAPK cascade induced by FGFs in fibroblast [19]. These indicate that significant antagonistic interplay may also occur between the CNP/GC-B pathway and growth factor-regulated pathways in growth plate chondrocytes.

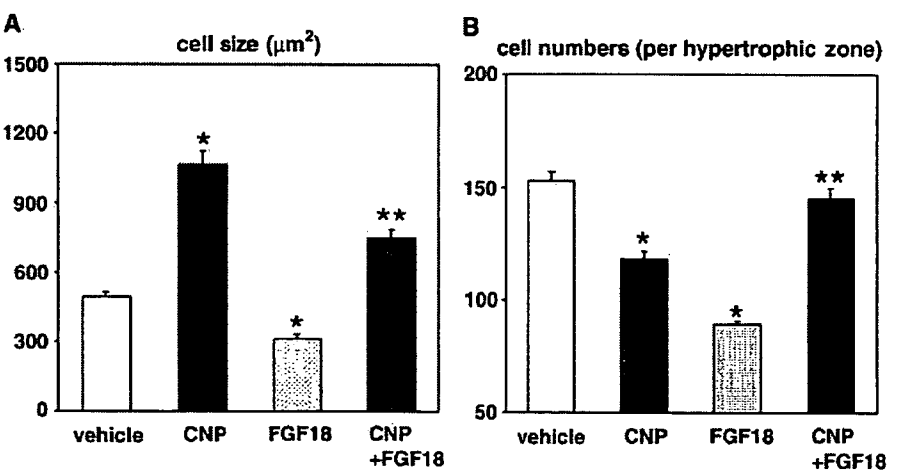

Fig. 7. Effect of CNP and FGF18 on mouse fetal tibia organ culture. (A) Effect of CNP and FGF18 on the size of hypertrophic chondrocytes (n = 10). Columns represent means ± SE (n = 10, each), $^{*}P < 0.01$ vs. vehicle, $^{**}P < 0.01$ vs. FGF18. (B) Effect of CNP and FGF18 on the numbers of hypertrophic chondrocytes (n = 5). Columns represent means ± SE (n = 5, each), $^{*}P < 0.01$ vs. vehicle, $^{**}P < 0.01$ vs. FGF18.

Constitutive activation of FGFR-3 has been reported to inhibit the proliferation and differentiation of the growth plate chondrocytes [20]. Our study clarified that CNP can undo the reduction in the size and numbers of chondrocytes of the hypertrophic zone of the growth plate of mouse tibias expressing the type X collagen, and compensate for the shortening of the growth plate resulting from the treatment with FGF18. These results are consistent with the findings of previous in situ hybridization studies which have shown that the mouse *fgfr-3* gene is widely expressed in the proliferative and prehypertrophic chondrocyte zones of cartilage [20], thus, overlapping the CNP/GC-B expression described in a previous study of ours [3]. Therefore, the interaction between the CNP/GC-B and FGFR-3 pathways in these cells results in the change of the hypertrophic chondrocytes during the endochondral ossification in the growth plate.

These findings, together with the fact that the specific MAPK inhibitors eliminated the FGF2-inhibition of CNP-dependent cGMP production in ATDC5 cells, suggest that the CNP/GC-B pathway and MAPK pathway counteracts through FGFR-3 in the regulation of growth plate chondrocytes.

Alternatively, one can hypothesize that the MAPK pathway is not the only FGFR-3 signaling pathway in chondrocytes. It has been suggested that the inhibitory effects of FGFs on bone growth are mediated by the STAT-1 pathway of FGFR-3 signaling [21], while a highly controlled balance between the MAPK and STAT-1 pathways has been demonstrated recently in growth factor-stimulated cells. The observation that the *Stat-1* null mice with overexpressing FGF2 can overcome apoptosis and the reduction in chondrocyte proliferation gives support to the view that the Stat-1 pathway may also have a key function in growth retardation [22]. In keeping with these findings, however, our observation of a significant ligand-independent STAT-1 phosphorylation in ATDC5 cells and no change in the level of STAT-1 phosphorylation as a result of stimulation by FGFs, CNP, or cGMP, leads us to conclude that the mechanism by which CNP undoes the shortening of bone length treated by FGFs consists of overcoming the MAPK-mediated pathway, not the STAT-1-mediated pathway.

Constitutive activation of ERK1 in chondrocytes reportedly induces a condition resembling achondroplasia [23]. Many studies have shown that activating mutations in FGFR-3 inhibit bone growth in patients with achondroplasia and thanatophoric dysplasia [24,25], while overexpression of FGF2 in mice slows longitudinal growth [26] and inactivating knockout mutations in FGFR-3 increase longitudinal long bone growth in mice [5]. On the other hand, CNP null mice as well as GC-B null mice are characterized by short stature with a phenotype histologically similar to that of achondroplasia [27]. Recently, we have shown that achondroplasia model mice, expressing the constitutive active mutant form of FGFR-3 (G380R) in cartilage [5], recovered from abnormal growth plate development and dwarfing phenotype as a result of the overexpression of CNP in their cartilage [28], suggesting that interaction between the CNP/GC-B and FGFR-3 pathways also occurs in vivo. Although two pathways are antagonistic, the effect of the CNP/GC-B pathway can overcome the effect of FGFR-3 pathway, partly because the activation level of downstream signaling of FGFR-3 (G380R) mutant is relatively weak [26], compared to the overexpressed CNP. During the course of this study, mutations in the human GC-B gene were reported to cause acromesomelic dysplasia, type Maroteaus, a type of skeletal dysplasia [29]. Therefore, the CNP/GC-B pathway appears critical for the proper progression of endochondral ossification also in human bone.

The downstream of the interaction between CNP/GC-B/cGMP pathway and FGFR-3/MAPK pathway remains unexplored. We recently reported that cGMP-dependent kinase depleted mice ($Prkg2^{-/-}$) showed abnormal growth plate development and dwarfing phenotype, that these changes were not affected by the overexpression of CNP in cartilage [30] and that the growth plate chondrocyte differentiation was disorganized, which is different from what has been observed in CNP-depleted mice.

GC-B is constitutively phosphorylated while receptor phosphorylation is absolutely essential for hormonal activation. On the other hand, the dephosphorylation of GC-B in response to hormone binding has been shown to correlate with the declining activity of these receptors in whole cells, suggesting that receptor dephosphorylation mediates the homologous desensitization of the receptor [31]. As the expression level of GC-B was not changed by FGF18 stimulation in our study, this dephosphorylation process may be involved in the desensitization of GC-B after FGFR-3 stimulation.

The clearance receptor of the natriuretic peptide reportedly mediates antimitogenic action of CNP in some but not all cell lines [32]. To determine if the effects of CNP were mediated by the clearance receptor in the ATDC5 cells, C-ANF, a selective ligand for the clearance receptor, was tested on ATDC5 cells and did not inhibit basal or FGF-stimulated ERK1/2 phosphorylation (data not shown).

We have demonstrated that the CNP/GC-B pathway engages in negative cross talks with FGFR pathways, that FGFs reduce CNP-dependent intracellular cGMP production and that CNP and cGMP markedly diminish the FGF-induced phosphorylation of ERK1/2 in chondrocytes. We also showed that CNP does not affect the amount of phosphorylated STAT-1 in chondrocytes. The results of our study show that FGFs and the activity of MAPK play an important role in the growth of chondrocytes, and negatively interact with the CNP/GC-B pathway and explain one of the molecular mechanisms of the growth stimulating action of CNP, suggesting that activation of the CNP/GC-B pathway may be effective for the treatment of achondroplasia.

Acknowledgments

This work was in part supported by Grant-in-Aid from The Ministry of Health, Labour and Welfare (#1028009) and the grant from the Smoking Research Foundation.

References

[1] Nakao K, Ogawa Y, Suga S, Imura H. Molecular biology and biochemistry of the natriuretic peptide system: I. natriuretic peptides. J Hypertens 1992;10:907–12.
[2] Nakao K, Ogawa Y, Suga S, Imura H. Molecular biology and biochemistry of the natriuretic peptide system: II. natriuretic peptide receptors. J Hypertens 1992;10:1111–4.
[3] Chusho H, Tamura N, Ogawa Y, Yasoda A, Suda M, Miyazawa T, et al. Dwarfism and early death in mice lacking C-type natriuretic peptide. Proc Natl Acad Sci USA 2001;98:4016–21.
[4] Yasoda A, Ogawa Y, Suda M, Tamura N, Mori K, Sakuma Y, et al. Natriuretic peptide regulation of endochondral ossification. Evidence for possible roles of the C-type natriuretic peptide/guanylyl cyclase-B pathway. J Biol Chem 1998;273:11695–700.
[5] Colvin JS, Bohne BA, Harding GW, McEwen DG, Ornitz DM. Skeletal overgrowth and deafness in mice lacking fibroblast growth factor receptor 3. Nat Genet 1996;4:390–7.
[6] Kanai M, Goke M, Tsunekawa S, Podolsky DK. Signal transduction pathway of human fibroblast growth factor receptor 3. Identification of a novel 66-kDa phosphoprotein. J Biol Chem 1997;272:6621–8.
[7] Deng C, Wynshaw-Boris A, Zhou F, Kuo A, Leder P. Fibroblast growth factor receptor 3 is a negative regulator of bone growth. Cell 1996;84:911–21.
[8] Tavormina PL, Rimoin DL, Thompson LM, Zhu YZ, Wilkin DJ, Lachman RS, et al. Thanatophoric dysplasia (type I and II) caused by distinct mutations in fibroblast growth factor receptor 3. Nat Genet 1995;9:321–8.
[9] Shimizu A, Tada K, Shukunami C, Hiraki Y, Kurokawa T, Magane N, et al. A novel alternatively spliced fibroblast growth factor receptor 3 isoform lacking the acid box domain is expressed during chondrogenic differentiation of ATDC5 cells. J Biol Chem 2001;276: 11031–40.
[10] Ellsworth JL, Berry J, Bukowski T, Claus J, Feldhaus A, Holderman S, et al. Fibroblast growth factor-18 is a trophic factor for mature chondrocytes and their progenitors. Osteoarthr Cartil 2002;10:308–20.
[11] Ohbayashi N, Shibayama M, Kurotaki Y, Imanishi M, Fujimori T, Itoh N, et al. FGF18 is required for normal cell proliferation and differentiation during osteogenesis and chondrogenesis. Genes Dev 2002; 16:870–9.
[12] Liu Z, Xu J, Colvin JS, Ornitz DM. Coordination of chondrogenesis and osteogenesis by fibroblast growth factor 18. Genes Dev 2002; 16:859–69.
[13] Shukunami C, Shigeno C, Atsumi T, Ishizeki K, Suzuki F, Hiraki Y. Chondrogenic differentiation of clonal mouse embryonic cell line ATDC5 in vitro: differentiation-dependent gene expression of parathyroid hormone (PTH)/PTH-related peptide receptor. J Cell Biol 1996;133:457–68.
[14] Suda M, Tanaka K, Yasoda A, Komatsu Y, Chusho H, Miura M, et al. C-type natriuretic peptide/guanylate cyclase B system in ATDC5 cells, a chondrogenic cell line. J Bone Miner Metab 2002;20:136–41.
[15] Tamura N, Garbers DL. Regulation of the guanylyl cyclase-B receptor by alternative splicing. J Biol Chem 2003;278:48880–9.
[16] Miura M, Tanaka K, Komatsu Y, Suda M, Yasoda A, Sakuma Y, et al. Thyroid hormones promote chondrocyte differentiation in mouse ATDC5 cells and stimulate endochondral ossification in fetal mouse tibias through iodothyronine deiodinases in the growth plate. J Bone Miner Metab 2002;17:443–54.
[17] Hotokezaka H, Sakai E, Kanaoka K, Saito K, Matsuo K, Kitaura H, et al. U0126 and PD98059, specific inhibitors of MEK, accelerate differentiation of RAW264.7 cells into osteoclast-like cells. J Biol Chem 2002;277:47366–72.
[18] Komatsu Y, Itoh H, Suga S, Ogawa Y, Hama N, Kishimoto I, et al. Regulation of endothelial production of C-type natriuretic peptide in coculture with vascular smooth muscle cells. Role of the vascular natriuretic peptide system in vascular growth inhibition. Circ Res 1996;78:606–14.
[19] Chrisman TD, Garbers DL. Reciprocal antagonism coordinates C-type natriuretic peptide and mitogen-signaling pathways in fibroblasts. J Biol Chem 1999;274:4293–9.
[20] Naski MC, Colvin JS, Coffin JD, Ornitz DM. Repression of hedgehog signaling and BMP4 expression in growth plate cartilage by fibroblast growth factor receptor 3. Development 1998;125:4977–88.
[21] Sahni M, Ambrosetti DC, Mansukhani A, Gertner R, Levy D, Basilico C. FGF signaling inhibits chondrocyte proliferation and regulates bone development through the STAT-1 pathway. Genes Dev 1999; 13:1361–6.
[22] Sahni M, Raz R, Coffin JD, Levy D, Basilico C. STAT1 mediates the increased apoptosis and reduced chondrocyte proliferation in mice overexpressing FGF2. Development 2001;128:2119–29.
[23] Murakami S, Balmes G, McKinney S, Zhang Z, Givol D, de Crombrugghe B. Constitutive activation of MEK1 in chondrocytes causes Stat1-independent achondroplasia-like dwarfism and rescues the Fgfr3-deficient mouse phenotype. Genes Dev 2004;18:290–305.
[24] Shiang R, Thompson LM, Zhu YZ, Church DM, Fielder TJ, Bocian M, et al. Mutations in the transmembrane domain of FGFR3 cause the most common genetic form of dwarfism, achondroplasia. Cell 1994; 78:335–42.
[25] Webster MK, D'Avis PY, Robertson SC, Donogue DJ. Profound ligand-independent kinase activation of fibroblast receptor 3 by the activation loop mutation responsible for a lethal skeletal dysplasia, thanatophoric dysplasia type II. Mol Cell Biol 1996;16:4081–7.
[26] Coffin JD, Florkiewicz RZ, Neumann J, Mort-Hopkins T, Dorn II GW, Lightfoot P, et al. Abnormal bone growth and selective translational regulation in basic fibroblast growth factor (FGF-2) transgenic mice. Mol Biol Cell 1995;6:1861–73.
[27] Tamura N, Doolittle LK, Hammer RE, Shelton JM, Richardson JA, Garbers DL. Critical roles of the guanylyl cyclase B receptor in endochondral ossification and development of female reproductive organs. Proc Natl Acad Sci USA 2004;101:17300–5.
[28] Yasoda A, Komatsu Y, Chusho H, Miyazawa T, Ozasa A, Miura M, et al. Overexpression of CNP in chondrocytes rescues achondroplasia through a MAPK-dependent pathway. Nat Med 2004;10:80–6.
[29] Bartels CF, Bukulmez H, Padayatti P, Rhee DK, van Ravenswaaij-Arts C, Pauli RM, et al. Mutations in the transmembrane natriuretic peptide receptor NPR-B impair skeletal growth and cause acromesomelic dysplasia, type Maroteaux. Am J Hum Genet 2004;75: 27–34.
[30] Miyazawa T, Ogawa Y, Chusho H, Yasoda A, Tamura N, Komatsu Y, et al. Cyclic GMP-dependent protein kinase II plays a critical role in C-type natriuretic peptide-mediated endochondral ossification. Endocrinology 2002;143:3604–10.
[31] Abbey SE, Potter LR. Lysophosphatidic acid inhibits C-type natriuretic peptide activation of guanylyl cyclase-B. Endocrinology 2003;144:240–6.
[32] Komatsu Y, Itoh H, Suga S, Igaki T, Ogawa Y, Kishimoto I, et al. Regulation of secretion and clearance of C-type natriuretic peptide in the interaction of vascular endothelial cells and smooth muscle cells. J Hypertens 1996;14:585–92.

Osteoporos Int (2006) 17: 105–108
DOI 10.1007/s00198-005-1923-3

ORIGINAL ARTICLE

High-dose glucocorticoid treatment induces rapid loss of trabecular bone mineral density and lean body mass

**Koshi Natsui · Kiyoshi Tanaka · Michio Suda
Akihiro Yasoda · Yoko Sakuma · Ami Ozasa
Shoichi Ozaki · Kazuwa Nakao**

Received: 11 December 2004 / Accepted: 5 April 2005 / Published online: 11 May 2005

Abstract A recent large-scale study revealed that glucocorticoid treatment increased fracture risk, which occurred at a far smaller dose and by a shorter duration than previously thought. To study the underlying mechanism for the increased risk of fracture, we studied the early changes in bone mineral density (BMD) and body composition by dual energy X-ray absorptiometry (DXA) after initiating high-dose glucocorticoid treatment. High-dose glucocorticoid treatment was arbitrarily defined as daily doses of ≥40 mg of a predonisolone equivalent. The 33 patients enrolled in this study had not received glucocorticoid treatment before. Only 2 months of treatment resulted in substantial BMD loss, most markedly in the lumbar spine, followed by the femoral neck and total body, which suggests the preferential trabecular bone loss. Body composition was also greatly affected. Thus, 2-month treatment with glucocorticoid significantly reduced bone mineral content (BMC), lean body mass (LBM) and increased fat mass (FAT). Our results are likely to have some clinical relevance. First, BMD loss occurs quite rapidly after starting glucocorticoid treatment, and patients receiving glucocorticoid treatment should be more carefully monitored for their BMD. Second, LBM, which mainly represents muscle volume, decreases rapidly after initiating glucocorticoid treatment. Decreased LBM might be also responsible for the increased risk of fracture, since falling is a well-known risk factor for fracture, and patients receiving glucocorticoid treatment should also be evaluated for their body composition.

Keywords Body composition · Dual energy X-ray absorptiometery · Glucocorticoid-induced osteoporosis · Lean body mass · Steroid myopathy

K. Natsui (✉)
Department of Medicine,
Fukui Red Cross Hospital, 4-2-1 Tsukimi,
918-8501 Fukui, Japan
E-mail: IBZ00745@nifty.ne.jp
Tel.: +81-776-363630
Fax: +81-776-364133

K. Tanaka
Department of Food and Nutrition,
Kyoto Women's University, Higashiyama,
Kyoto, Japan

M. Suda
Department of Endocrinology, Kyoto City Hospital,
Nakagyo, Kyoto, Japan

A. Yasoda · Y. Sakuma · A. Ozasa · K. Nakao
Department of Endocrinology and Metabolism,
Kyoto University Hospital, Sakyo, Kyoto, Japan

S. Ozaki
Division of Rheumatology and Allergy,
St. Marianna University School of Medicine,
Kawasaki, Japan

Introduction

Among the various adverse events associated with therapeutic glucocorticoid use, osteoporotic fracture is considered to be the most common complication [1]. A large-scale study from the UK clearly demonstrated that glucocorticoid treatment, even with small dosage and for short duration, significantly increased the risk of fracture [2]. Furthermore, a recent meta-analysis by van Staa et al. showed that the risk of fracture increased quite rapidly (within 3 to 6 months) after initiating the glucocorticoid treatment [3]. Prompted by these works, we have studied the early effects of high-dose glicocorticoid use on the skeletal system.

The purpose of this paper was twofold: first, to examine the initial effects of glucocorticoid on bone mineral density (BMD) at various skeletal sites; second, to study the effects of glucocorticoid on body composition based on the following considerations. Recent evidence suggests that the fracture threshold in patients with glucocorticoid-induced osteoporosis (GIO) is different from that in patients with primary osteoporosis [4]. Although glucocorticoid is known to cause muscle

weakness called "steroid myopathy" [5], far less attention has been paid to this condition than GIO. We suspected that myopathy and increased risk of falling might also be responsible for the increased risk of fracture. The patients included in this study received glucocorticoid treatment for the first time, and the patients that received higher doses of glucocorticoid were exclusively studied. The protocol was so determined because we considered that it is a suitable model to study the initial effects of high-dose glucocorticoid on the musculoskeletal system.

Materials and methods

Thirty-three patients hospitalized at the Kyoto University Hospital and scheduled to receive intensive glucocorticoid therapy were recruited in this study (Table 1). None of the patients had received glucocorticoid treatment before. Five patients were male (54.0 ± 7.6 years old), and 28 were female (38.9 ± 16.4 years old). "Intensive glucocorticoid therapy" was arbitrarily defined as the daily dose of glucocorticoid ≥40 mg of predonisolone equivalent. Nineteen patients received intravenous pulse treatment followed by oral glucocorticoid treatment. Fourteen patients received only oral glucocorticoid treatment. Their underlying diseases are as follows, with the number of subjects in parentheses: Graves' ophthamopathy (8), dermatomyositis (DM), polymyositis (PM) and mixed connective disorder (MCTD) (9), systemic lupus erythematodes (SLE) (16) and nephrotic syndrome (NS) [2]. Bone mineral density (BMD) and body composition were measured before and 2 months after initiating the glucocorticoid therapy. These measurements were performed with dual energy X-ray absorptiometry (DXA) (QDR-2000; Hologic, Waltham, Mass.) by a single examiner. BMDs were measured for the lumbar spine (L2–4), femoral neck and whole body. From the whole body measurement, the following parameters of body composition were obtained: lean body mass (LBM), fat mass (FAT) and bone mineral content (BMC).

Table 1 Patient characteristics

Number of patients	33		
Sex and age	Male	5	(54.0 ± 7.6 years old)
	Female	28	(38.9 ± 16.4 years old)
Underlying diseases	Systemic lupus erythematosus	(16)	
	Myositis	(9)	
	Graves' opthalmopathy	(8)	
Route of administration	Intravenous pulse + oral	(19)	
	Oral	(14)	

Results

High-dose glucocorticoid treatment for 2 months caused significant BMD loss at all three sites measured in the present study (Table 2). Of these three sites, the lumbar spine showed the greater percentage of BMD loss (–2.87%) compared to the femoral neck (–1.37%) and whole body (–1.10%). These differences were highly statistically significant by Fisher's PLSD.

The effect of high-dose glucocorticoid treatment on body composition was also studied (Table 3A). Two cases with nephrotic syndrome were excluded from the statistical analysis because the existence of severe edema is likely to interfere with the measurement of body composition. The initial body mass index (BMI) of the patients was 20.07 ± 3.06 kg/m^2, which did not significantly deviate from the standard BMI value of 22. Intensive glucocorticoid treatment for 2 months significantly decreased the BMI to 19.19 ± 2.83 kg/m^2 ($P < 0.05$).

BMC and LBM significantly decreased after glucocorticoid treatment (Table 3A). In contrast, fat mass (FAT) significantly increased. When expressed as %FAT, that is the ratio of FAT divided by body weight, the change was more pronounced. Thus, %FAT before treatment was 22.72 ± 6.22%, and it increased to 25.26 ± 5.65% after treatment ($P < 0.001$).

To exclude possible interference by the pre-existing myositis, data were also analyzed in 24 patients, excluding the cases with muscle involvement (DM/PM/MCTD) (Table 3B). The results were similar to the ones from the whole 33 cases. Thus BMI, BMC and LBM significantly decreased after the treatment. Although FAT after treatment was not statistically different from the pre-treatment value, %FAT after treatment was significantly higher than that before treatment.

The total dosage of glucocorticoid within 2 months ranged from 1,000 to 4,000 mg in cases with oral glucocorticoid treatment, and from 4,500 to 12,000 mg in cases with intravenous pulse treatment. Total glucocorticoid dosage correlated with none of the parameters in the present study, such as BMI, LBM and fat mass (data not shown).

Discussion

Recently, van Staa et al. clearly demonstrated that glucocorticoid use is a significant risk factor for both vertebral and nonvertebral fractures [2]. Their study is an exceptionally large-scale study from the UK including over 240,000 subjects in both control and glucocorticoid groups. Their reports have some important clinical implications. First, they found that even a small dosage of glucocorticoid use for a short duration of time significantly increased the risk of fracture. Until recently, glucocorticoid use was considered to be a risk factor for osteoporosis when the average daily dosage was greater

Table 2 Changes in bone mineral density after 2 months of high-dose glucocorticoid treatment

	Pretreatment	Post-treatment	*P* value
Lumbar spine (L2–4)	0.94 ± 0.17	0.91 ± 0.17	< 0.0001
Femoral neck	0.735 ± 0.123	0.725 ± 0.125	< 0.01
Whole body	1.031 ± 0.111	1.019 ± 0.111	< 0.001

than or equal to the predonisolone equivalent of 7.5 mg and the duration was > 6 months [6]. According to van Staa et al., however, fracture risk was already increased at as early as 3 months after starting the glucocorticoid treatment, and even a daily dosage of less than 2.5 mg predonisolone equivalent was associated with increased risk of vertebral fracture [2]. Another important implication was that glucocorticoid treatment was unequivocally proven to be a risk factor for fracture. The current concept holds that the reduction of fracture risk should be the endpoint in the treatment of osteoporosis, the increase of BMD being only a surrogate endpoint [7]. Thus, it is a landmark study in that fracture was the endpoint in the study of GIO.

In the current study, only 2 months of high-dose glucocorticoid treatment markedly decreased BMD in all three sites measured: the lumbar spine, femoral neck and whole body. The BMD decrease was the greatest in the lumbar spine compared to the femoral neck and whole body. These differences are likely to be due to the variable composition of each bone [8]. Thus, the lumbar spine is mainly composed of trabecular bone, and both cortical and trabecular bones contribute to the femoral neck BMD. Since approximately 70% of total bone volume is composed of cortical bone, cortical bone volume is the major determinant of total body BMD. Therefore, these results suggest that trabecular bone is mainly affected by intensive glucocorticoid treatment, which is in accordance with the previous reports [6].

Although glucocorticoid affects various aspects of skeletal homeostasis, its major effect is considered to be the suppression of bone formation, which is mainly exerted through inducing apoptosis in osteoblasts and osteocytes, and suppressing local IGF-1 production [9, 10]. Although glucocorticoid is known to decrease intestinal calcium absorption, the effect is usually only modest and does not cause marked secondary hyperparathyroidism. Glucocorticoid also increases urinary calcium excretion by inhibiting tubular calcium reabsorption. With regard to bone resorption, glucocorticoid treatment is reported to enhance bone resorption transiently by inducing RANKL and suppressing OPG [9, 10].

Despite the significant detrimental effects of glucocorticoid on BMD, it is not likely to be the sole explanation for the glucocorticoid-induced increase in the fracture rate. The fracture risk in GIO has been reported to be either altered [11] or unaltered [12]. A recent paper by Wallch, however, strongly favors the notion that fracture occurs at higher BMD values in GIO than in postmenopausal osteoporosis [4]. In their report, which is part of the risedronate trial on GIO, the vertebral fracture rate was as high as 16%, whereas lumbar BMD was only modestly decreased, the average T score being −1.2. Van Staa et al. suggested three mechanisms for the increased fracture rate in GIO [2]: the apoptosis of osteoblasts and osteocytes, the marked alteration in bone turnover and non-skeletal mechanisms such as falling. Glucocorticoid is known to alter the body composition greatly. Muscle weakness called "steroid myopathy" and central obesity are well-known complications of glucocorticoid treatment [5], and muscle weakness is by no doubt one of the major risk factors of falling. In this study, body composition was evaluated by DXA, since it is considered to be a standard method for the evaluation of body composition as well as for BMD measurement [13]. LBM significantly decreased, and FAT increased in a reciprocal fashion in within only 2 months, Therefore, the percentage of fat (%FAT) increased by approximately 10%. Although vertebral fracture, which is the most prevalent fracture in GIO, is not associated with falling [10], an increased rate of falling would lead to the increased risk of hip and wrist fractures. Thus, our current finding may explain at least partially the increased fracture risk in glucocorticoid treatment.

Another implication of the current findings would be the rapidity with which bone loss occurs after initiating

Table 3 Changes in body composition after 2 months of high-dose glucocorticoid treatment. *A* and *B* show the data from whole subjects and data from patients excluding ones with myositis, respectively. BMC, LBM and FAT are expressed in kg. %FAT is the ratio of fat to body weight

	Pretreatment	Post-treatment	*P* value
A			
Body mass index (BMI)	20.07 ± 3.06	19.19 ± 2.83	< 0.05
Body composition			
Bone mineral content (BMC)	1.94 ± 0.38	1.88 ± 0.37	< 0.001
Lean body mass (LBM)	37.30 ± 6.80	34.26 ± 5.00	< 0.0001
Fat mass (FAT)	11.66 ± 4.00	12.47 ± 3.95	< 0.05
%FAT	22.72 ± 6.22	25.26 ± 5.65	< 0.001
B			
Body mass index (BMI)	20.00 ± 3.37	19.28 ± 3.05	< 0.05
Body composition			
Bone mineral content (BMC)	1.89 ± 0.34	1.84 ± 0.33	< 0.001
Lean body mass (LBM)	35.52 ± 6.37	33.33 ± 4.79	< 0.005
Fat mass (FAT)	12.03 ± 4.51	12.44 ± 4.22	NS
% FAT	23.89 ± 6.75	25.60 ± 6.22	< 0.05

intensive glucocorticoid treatment. It is now established that even low dose glucocorticoid treatment increases the fracture risk. Vestergaard et al. reported that even a limited daily dose of glucocrticoid (more than an average dose of 71 μg predonisolone per day) was associated with an increased risk of hip fracture [14]. In the guideline for GIO recently published by the UK, it is recommended that BMD measurement should be considered for patients committed or exposed to oral glucocorticoid for more than 3 months, irrespective of the glucocorticoid dose [15]. These reports, together with the current findings, strongly suggest that attention should be paid to the prevention as well as the treatment of GIO.

These changes are unlikely to be secondary to hospitalization or due to underlying disease alone. First, increased %FAT in face of decreased body weight is quite unlikely to occur as the result of underlying disease or the subsequent malnutrition. Moreover, when the subgroup of patients with euthyroid Graves' disease was separately analyzed, these changes in body composition and biochemical parameters were similarly observed (data not shown). These patients have inflammatory changes only in their extraocular muscle and do not have any limitation in their daily activities except for double vision. Therefore, these marked changes are probably due to the intensive glucocorticoid treatment rather than other factors. Additionally, the patients' BMD was not markedly decreased before treatment. Since reference data for whole body BMD using QDR-2000 in the Japanese population is not available, we have not expressed our data in Z score. The young adult mean (YAM) for lumbar spine BMD in Japanese women is 1.011 ± 0. The YAM for the femoral neck BMD is 0.787 ± 0.109 for women and 0.863 ± 0.127 for men. Thus, it is quite unlikely that underlying diseases had adversely affected the subjects' skeletons before glucocorticoid treatment.

In summary, we have shown that intensive glucocorticoid treatment rapidly induces trabecular bone loss and lean body mass, both of which probably contribute to the recently reported rapid onset of increased fracture risk after initiating glucocorticoid treatment.

References

1. Saag KG, Koehnke R, Caldwell JR, Brasington R, Burmeister LF, Zimmerman B, Kohler JA, Furst DE (1994) Low dose long-term corticosteroid therapy in rheumatoid arthritis: an analysis of serious adverse events. Am J Med 96:115–123
2. van Staa TP, Leufkens HGM, Abenhaim L, Zhang B, Cooper C (2000) Use of oral corticosteroid and risk of fractures. J Bone Miner Res 15:993–1000
3. van Staa TP, Leufkens HG, Cooper C (2002) The epidemiology of corticosteroid-induced osteoporosis: a meta-analysis. Osteoporos Int 13:777–787
4. Wallach S, Cohen S, Reid DM, Hughes RA, Hosking DJ, Laan RF, Doherty SM, Maricic M, Rosen C, Brown J, Barton I, Chines AA (2000) Effects of risedronate treatment on bone density and vertebral fracture in patients on corticosteroid therapy. Calcif Tissue Int 67:277–285
5. Kanda F, Okuda S, Matsushita T, Takatani K, Kimura KI, Chihara K (2001) Steroid myopathy: pathogenesis and effects of growth hormone and insulin-like growth factor-I administration. Horm Res 56:S24–S28
6. American College of Rheumatology Task Force on Osteoporosis Guidelines (1996) Recommendations for the prevention and treatment of glucocorticoid-induced osteoporosis. Arth Rheum 39:1791–1801
7. Pearson D, Miller CG (eds) (2002) Clinical trials in osteoporosis. Springer, Heidelberg Germany New York
8. Bonnick SL, Lewis LA (2002) Bone densitometry for technologists. Humana Press, Totowa, NJ
9. Canalis E, Giustina A (2001) Glucocorticoid-induced osteoporosis: summary of a workshop. J Clin Endocrinol Metab 86:5681–5685
10. Canalis E, Delany AM (2002). Mechanism of glucocorticoid action in bone. Ann NY Acad Sci 966:73–81
11. Luengo M, Picado C, Del Rio L, Guanabens N, Monsterrat JM, Setoain J (1991) Vertebral fractures in steroid dependent asthma and involutional osteoporosis. Thorax 46:803–806
12. Selby PL, Halsey JP, Adams KRH, Klimiuk P, Knight SM, Pal B, Stewart IM, Swinson DR (2000) Corticosteroids do not alter the threshold for vertebral fracture. J Bone Miner Res 15:952–956
13. Houtkooper LB, Going SB, Sproul J, Blew RM, Lohman TG (2000) Comparison of methods for assessing body-composition changes over 1 year in postmenopausal women. Am J Clin Nutr 72:401–406
14. Vestergaard P, Olsen ML, Paaske Johnsen S, Rejnmark L, Toft Sorensen H, Mosekilde L. (2003) J Intern Med 254:486–493
15. Bone and Tooth Society, National Osteoporosis Society, Royal College of Physicians. (2002) Glucocorticoid-induced osteoporosis: guidelines for prevention and treatment. Royal College of Physicians, London